Alma Mater Studiorum · Università di Bologna

Scuola di Scienze

Corso di Laurea Magistrale in Fisica

The FOOT Experiment: the Associated Physics and its Acquisition System.

Relatore:
Prof. Mauro Villa
Correlatrice:
Dott.ssa Silvia Biondi

Presentata da:
Chiara De Lucia

III Sessione
Anno Accademico 2016/2017

"Alle prime volte e alle ultime cose.
Agli inizi e alle conclusioni.
Al disagio, alle tende, ai campeggi.
Allo zaino e al suo essere pesante, ma leggero.

A chi è solo passato e a chi è rimasto.
A chi ha condiviso giorni e a chi notti.
A chi ha smezzato una birra e a chi cento.
A chi c'è stat per un passo, un sentiero o l'intero cammino."*

Ma soprattutto a te, Bologna,
per avermi lasciato scegliere chi voglio essere.

Sommario

Secondo l'organizzazione mondiale della sanità, nel 2015 le morti causate da tumori sono state circa 8.8 milioni. Ogni tumore necessita di un trattamento specifico detto "Treatment Planning System (TPS)", il quale non è completo per l'adroterapia, in quanto i dati che riguardano la dose di radiazione rilasciata nel paziente non sono sufficienti per stimare un giusto valore di efficacia biologica (RBE, Relative Biological Effectiveness), tenendo conto della dose del fascio stesso e delle particelle prodotte dalla frammentazione del proiettile e del bersaglio.

In questo contesto, si colloca l'esperimento FOOT, progetto finaniato dall'INFN, in grado di raccogliere misure e dati sulle sezioni d'urto di frammentazione, sia di proiettile che del bersaglio. Infatti le informazioni a riguardo sono poche, soprattutto per le interazioni di protoni e ioni su materiali presenti nei tessuti umani, con fasci di energia usati in adroterapia (circa 250 MeV per i protoni e 350 MeV/n per gli ioni di Carbonio).

Al momento, l'esperimento FOOT è al suo inizio, così come l'apparato sperimentale e il sistema di acquisizione dati. Su queste basi, in questo lavoro di tesi si vuole riportare il panorama scientifico attuale, evidenziando la necessità di coprire i dati mancanti con nuove misure. Inoltre, è riportato un esempio preliminare di sistema di acquisizione dati con il rispettivo sistema di monitoraggio online per testare le schede elettroniche di acquisizione.

Abstract

According to the World Health Organization (WHO) about 8.8 million of deaths in 2015 were caused by cancer. The treatments for cancer are several: beyond the traditional surgery, chemiotherapy and radiotherapy, also hadrontherapy is developing. The hadrontherapy cures the cancer with ion or proton beams. Every tumor type requires a specific treatment plan called Treatment Planning System (TPS), that it is not complete for hadrontherapy because there is the need of knowing the dose deposition both due to the beam particle ionization and the fragmentation.

In this context, the FOOT experiment aims at collecting measurements and data about target or projectile fragmentation cross sections since currently the experimental panorama is rather scarse on the measurements of fragments produced in the interaction of protons or ions with tissue nuclei at the hadrontherapy energies (about 250 MeV for protons and 350 MeV/n for carbon ions).

At the moment, the FOOT experiment is at its start and so are the detectors setup and the acquisition system projects. On these bases, this thesis work reports the scientific panorama, highlighting the need of covering the measurement lacks. Moreover, a preliminary example of DAQ system is described with a connected online monitoring system to test the DAQ boards.

Contents

Introduction **1**

1 Hadrontherapy **3**

1.1 History of Hadrontherapy 3

1.2 Physics Principles in Hadrontherapy 7

1.2.1 The Bethe-Bloch formula and the Bragg peak 8

1.2.2 Nuclear fragmentation 11

1.3 Radiobiological Effects 13

1.3.1 Physical aspects 13

1.3.2 Biological aspects 14

1.4 Comparisons 19

1.4.1 Hadrontherapy and radiotherapy 19

1.4.2 Protons and ions 21

2 The FOOT Project **25**

2.1 Motivations of the Experiment 26

2.2 Experimental Strategies for Measurements 29

2.2.1 The inverse kinematic approach 30

2.2.2 Two different setups 32

2.3 FOOT Detector Setup 33

2.3.1 Heavy nuclei detection 34
2.3.2 Light nuclei detection 36

3 Fragmentation Cross Sections **39**
3.1 Cross Sections Measurement 40
3.2 Previous Data on Fragmentation 45
3.2.1 Proton beams 48
3.2.2 Carbon ion beams 54

4 The Acquisition System **63**
4.1 The DAQ Components 63
4.1.1 The trigger 67
4.1.2 The flash ADC 68
4.1.3 The vertex detector 69
4.2 The DAQ Interface 70
4.3 Event Building and Storage 73
4.3.1 The raw data files and event format 74
4.4 The Event Reading Code 76
4.4.1 The acquisition control code 81

Conclusions **83**

Bibliography **85**

Acknowledgements **90**

Introduction

Nearly one out of six deaths per year is due to cancer, which is the second leading cause of death globally and has been responsible for 8.8 million deaths only in 2015. Cancer, or tumor, is a generic term for a large group of diseases that can affect any part of the body. One of the main features of the cancer is the rapid creation of abnormal cells that grow beyond their usual boundaries, and which can invade adjoining parts of the body and spread to other organs (metastases). Every cancer type requires a specific treatment plan that encompasses one or more modalities such as surgery, radiotherapy, chemotherapy and, more recently, immunotherapy. In the last decades, the progress in technology has lead to the establishment of an alternative technique with respect to conventional radiotherapy, based on charged particle beams: hadrontherapy (or proton therapy).

The hadrontherapy is an oncological technique that exploits the different energy loss mechanism that characterizes the interaction of protons and other ions with matter (which is different with respect to the case of photons or electrons). Infact, charged particles release almost all the energy at the end of their path in tissues, in correspondence to the so called Bragg peak position, minimizing the damage to surrounding healthy tissues and organs at risk [1]. These physics aspect and radiobiological effects will be illustrated in Chapter 1, using them for comparing hadrontherapy with radiotherapy

and the use of protons with ions.

However, there is the pressing need of increasing the dose deposition knowledge due to the fragmentation of the incident particles (with the atomic number $Z > 1$) and the target tissues. Currently a very low number of experimental measurements of nuclear reaction cross sections of fragments produced in the interaction with tissues nuclei (especially H, C, O) of 60-250 MeV protons and 100-350 MeV/n carbon ions, which are the typical energies adopted in hadrontherapy treatments. These data are required to improve the algorithms currently used in the Treatment Planning Systems (TPS) for proton and heavy ion therapy, necessary to prepare the patient for the treatment procedure. The scientific scenario of all the measurements performed in this field will be summarized and shown in Chapter 3.

The main goal of the FOOT (FragmentatiOn Of Target) experiment is to measure the target and projectile fragmentation cross sections relevant for hadrontherapy. To achieve the goal, the FOOT experiment adopts an inverse kinematic approach to overcome the difficulties related to the short fragments range ($\sim \mu$m). Moreover, in order to bypass the problems given by the management of a pure hydrogen target, data are extracted by subtraction of cross sections on C and C_2H_4 targets. The FOOT detector and its setup will be discussed in Chapter 2.

The aim of the present thesis is to described the written algorithm for monitoring the Data Acquisition System (DAQ), discussed in Chapter 4. At the moment the acquisition system does not include all the devices for the whole detector, however it is important to preliminary check this with some tests, in particular regarding the main features and information as well performing acquisition system, as the event number for each device.

Chapter 1

Hadrontherapy

The "hadrontherapy" is an oncological technique that uses protons and ions as the main projectiles to kill cancer cells. It is a therapy complementary to the radiotherapy, that uses X-rays and gamma rays to threat patients, and that can be used also in situations where standard treatments like surgery, chemiotherapy or radiotherapy cannot be used. This happens in situations where the cancer cells are located in brain, in the spine or near organs that might suffer from other therapies. As an example, the hadrontherapy has been already used for almost 30,000 patients with a cancer near critic organs. In these case a standard radiotherapy, which is more invasive, would compromise the functionality of the close-by organs. In this chapter the main aspects of the hadrontherapy, its history, its working principles and applications are briefly recalled.

1.1 History of Hadrontherapy

More than a hundred years have passed since the discovery of X-rays by *William Conrad Röntgen* in 1895, who demonstrated the extraordinary

properties of his 'rays', which today we know to be photons of energy around 10^4 eV. Observing the absorption of X-rays, the conclusion was that different tissues have a different absorption coefficient for X-rays: this led to the first radiography (Fig.1.1).

Figure 1.1: The first radiography made by *Röntgen* .

Then, in 1896, *Henry Becquerel* discovered the natural radioactivity, and, even if the radiobiological effects were not known at that time, the idea to cure cancer with this mysterious radiations has been achieved.

The first application of accelerators in medicine started in 1931, thanks to the first cyclotron realized by *Ernest Lawrence* and *Stan Livingston*. Ernest and his brother John (a doctor, considered the founder of nuclear medicine) started to irradiate patients with salivary gland tumor using neutron beams; and since neutron nuclear products are ions this study can be considered the first use of ions for treating cancer.

The history of this new technique began in 1946 when *Robert Wilson*

was called to lead the team for the design and the construction of a new 160 MeV cyclotron in Harvard. He spent one year in Berkeley, collaborating with Ernest Lawrence, who had been his professor in the early 1930s, to complete the design of the accelerator. It was then that Lawrence asked him to define the shielding of the new cyclotron, by calculating the interactions with matter of a beam of 100 MeV protons. Wilson followed this suggestion and found that the proton dose has a completely different trend with depth than a beam of X-rays.

Infact, protons remove electrons from molecules, ionizing them while slowing down and the maximum number of ionisations per millimeter (placed at the end of the range) is called Bragg Peak.[1] These observations leaded Wilson to propose the use of protons for irradiating solid tumors, as a better therapy than the one based on X-rays. His pioneering and now famous paper ("Radiological Use of Fast Protons") was published in 1946 in the journal Radiology [2].

Two years after Wilson's paper, researchers at the Berkeley Laboratory conducted extensive studies on proton beams and confirmed his predictions. After many animal irradiations, the first patient was treated in 1954 under the guidance of *Cornelius Tobias*, a Hungarian physicist, who, together with Lawrence, performed the first hadron treatment on humans. The first irradiations were not directly on the tumor but on the pituitary gland that, after treatment, would stop making hormones that stimulated the cancer cells to grow. Patients with metastatic breast cancers were treated surgically to remove most of the tumoral mass and then irradiated with protons on the pituitary gland to reduce the production of grow hormones and hence the chances of metastatic proliferation. The pituitary gland was a natural site

[1] William Bragg was the first to discover the existence of this peak for alpha particles.

for the first treatments, because the gland location was easily identified with standard X-ray films. Between 1954 and 1974 about 1,000 hypophysis and pituitary tumors were treated with protons with a 50% success rate.

This technique was so called 'hadrontherapy' in 1992 and this term was later used to include all types of non-conventional radiation beams used at the time: protons, helium ions, neon ions, neutrons and pions. Indeed physicists call 'hadrons'[2] all the particles that feel the strong interaction because they are made of quarks and antiquarks [3].

The hadrontherapy is nowadays not widely uses compared with the radiotherapy due to two factors: space and cost. In case of radiotherapy, photons are produced by accelerated electrons up to 10 MeV, while protons (for hadrontherapy) needs to be accelerated to reach higher kinetic energies (up to 200 MeV) in order to have a suitable range in body to reach deep sited tumors, as 200 MeV. For these reasons cyclotrons and synchrotrons are so much more expensive than LINAC (Linear Accelerators) which are employed in radiotherapy. The hadrontherapy is not a substitution of radiotherapy, but it's useful to treat tumors that are "radio-resistance" or localized near an organ.

The kind of tumors that are mostly treated with hadrontherapy are *chordoma*[3] and *chondrosarcoma*[4], which are located in critic zones like the base of cranium or spine; *uveal melanoma*[5] for which the proton therapy produces the same chance of survival than the enucleation. In the first two cases, after a certain time, are free from tumor recurrencies is about 80%, instead of the 40% for patients treated with X-rays. For the uveal melanoma is more than

[2]From the greek *adrós* that means 'strong'.

[3]A rare malign tumor of the bone tissue.

[4]Different kind of tumors, they start from cartilage cells.

[5]It's the more frequent eye tumor in adults, it can make metastasis even after 20 year.

95% and more of 80% of patients that have kept the sight capability after treatment.

This and more results brought lots of oncologists to approve the superiority of the proton therapy, especially for children (because hadrontherapy has a less risk of induced carcinogenesis).

The evolution of hadrontherapy was not a process that developed only in the USA, but in the '80 a lot of hadrontherapy centers were built also in Japan. Recently also Italy has opened 3 national centers: CATANA (in Catania, where only eye tumors are treated), CNAO (in Pavia, where since 2011 they are using carbon ions for treatments) and the *Proton Therapy Center* (in Trento, that started to cure patients in 2014).

1.2 Physics Principles in Hadrontherapy

This section concerns the basic reactions which occur when heavy charged particles encounter matter and their effects. Heavy charged particles (with $M >> m_e$[6]) see matters in terms of electrons and nuclei, so processes that can occur are both elettromagnetic and nuclear. In general, two principal elettromagnetic features characterize the passage of charged particles, with a bigger mass than electrons, through matter: (1) a loss of energy by the particle (inelastic collisions with the atomic electrons), (2) a deflection of the particle from its incident direction (elastic scattering from nuclei).

These two reactions may occur many times per unit path length in matter, heavy particles may also interact directly with nuclei, though nuclear processes or reactions that might produce secondary particles [4].

While the single particle interactions can be described at the atomic or

[6]Where M is the mass of the particle and m_e the electron rest mass.

nuclear level, at the macroscopic level the most important quantity is the "stopping power" that parametrize the friction force that acts on an ion while it travel inside the medium. The stopping power that measure the energy loss per unit of path length depends on the properties of the charged particle such as its mass, charge, velocity and energy as well as on the properties of the absorbing medium such as its density and atomic number.

1.2.1 The Bethe-Bloch formula and the Bragg peak

The inelastic collisions with electrons are the principal responsible for the energy loss of the heavy charged particles in matter. In these processes the energy is transferred from the particles to the atomic electrons, causing and excitation (soft collision) or an ionization (hard collision). The amount of energy transferred in each collision is a small fraction of the particle's total kinetic energy; however the number of collisions per unit path lenght (in dense matter) is so large, that a substantial cumulative energy loss is observed.

Elastic scattering from nuclei also occurs frequently although not as often as electron collisions. In general the transferred energy in these collisions is smaller and negligible. In general, a sizeable fraction of energy is transferred in each single collision and its exact amount depends on the ratio of the impinging particle mass and the mass of the nuclei of the medium. The energy lost in this way is in any case a small fraction of the overall energy loss since the probability of nuclear scattering is much lower than the probability of interactions with the electrons.

So, during its motion through an absorbing medium, a charged particle experiences a large number of interactions before its kinetic energy is completely lost. In each interaction the charged particle's path may be altered

(elastic or inelastic scattering) and it may lose some of its kinetic energy that will be transferred to the medium. The energy loss of the charged particle propagating through the absorbing medium depends on the characteristics of the particle as well as the absorber; and each interaction has a specific cross section σ.

The rate of energy loss (typically expressed in MeV) per unit of path length (typically expressed in cm) by a charged particle in an absorbing medium is called the *linear stopping power* $(-\mathrm{d}E/\mathrm{d}x)$ [5]. The stopping power for heavy charged particles in matter was first calculated by *Bohr* using a classic approach and later by *Bethe* and *Bloch* using quantum mechanics. The formula obtained by Bethe, Bloch and other physicists is then:

$$-\frac{\mathrm{d}E}{\mathrm{d}x} = 2\pi N_A r_e^2 m_e c^2 \rho \frac{Z}{A}\frac{z^2}{\beta^2}\left[\ln\left(\frac{2m_e\gamma^2\nu^2 W_{max}}{I^2}\right) - 2\beta^2 - \delta - 2\frac{C}{Z}\right]$$

Here, there is a first constant part that depends from the classical electron radius ($r_e^2 = 2.817 \cdot 10^{-13}$ cm), the electron mass (m_e) and to the Avogadro's number ($N_A = 6.022 \cdot 10^{23}$ mol^{-1}). Then, there is a part depending on the medium characteristics (atomic number Z, atomic weight A and the density ρ) and a part depending on the beam characteristics: the charge of the incident particle (z, in unit of e), the mean excitation potential (I), the ratio v/c (β) and γ, the maximum energy transfer in a single collision (W_{max}).

The last two terms in the Bethe-Bloch Formula are two corrections: δ is the *density effect* correction and C the *shell* correction. The first is important at high energies and the second at low energies, so both are outside the range of energy that are important in hadrontherapy and can be neglected.

In the Figure 1.2 is shown the stopping power as function of the $\beta\gamma$ of the particle, that is equal to the ratio $\frac{p}{Mc}$, where p is the momentum of the particle, M the mass and c the light speed. For a non relativistic particle, $\mathrm{d}E/\mathrm{d}x$ is dominated by the overall factor $1/\beta^2$ and decreases with increasing

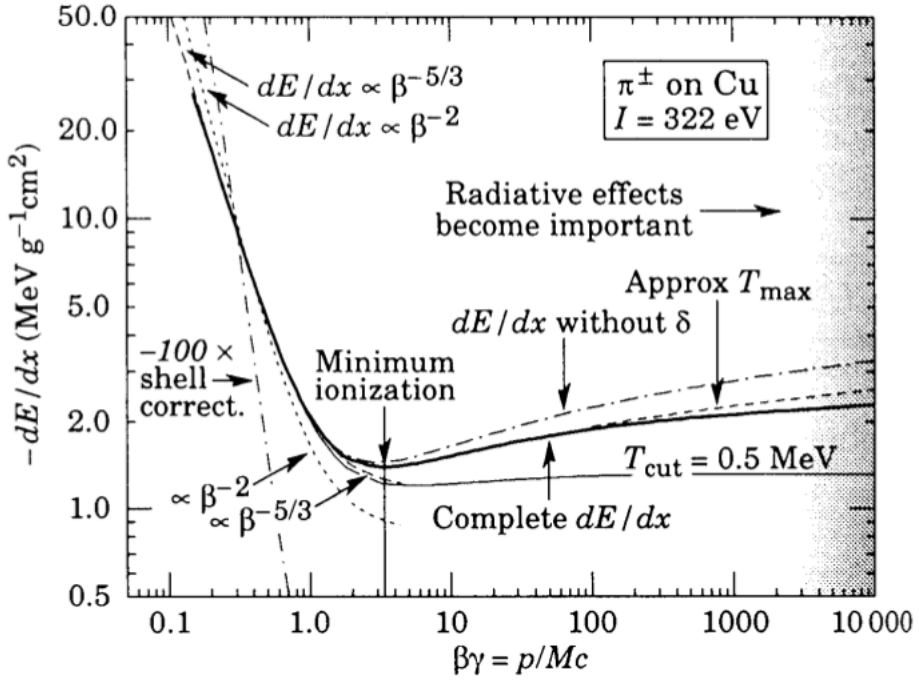

Figure 1.2: The linear stopping power divided by the density ρ of the medium (in unit of MeV cm^2 g^{-1}) in function of $\beta\,\gamma$ of the particle.

velocity until a minimum is reached at $v \sim 0.96c$. At this point, particles are usually referred to as Minimum Ionizing Particles (MIP). As the energy increases beyond the MIP point, dE/dx rises again due to the logarithmic contribution in Bethe-Bloch formula. When different charged projectiles with the same velocity are compared, z is the only factor that change outside the logarithmic term, so particles with greater charge will have a larger specific energy loss. Instead, studying dE/dx for different materials as absorbers, it can be pointed out its main dependence on the electron density of the medium: the higher is the density materials, the higher is the energy loss. Taking into account all the aforementioned considerations, a heavy charged particle deposits more energy per unit path length at the end of its path inside the target, rather than at its beginning, as shown in Figure 1.3. The

amount of ionization created by a heavy charged particle as a function of its penetration depth inside the target is known as the *Bragg Curve* [4].

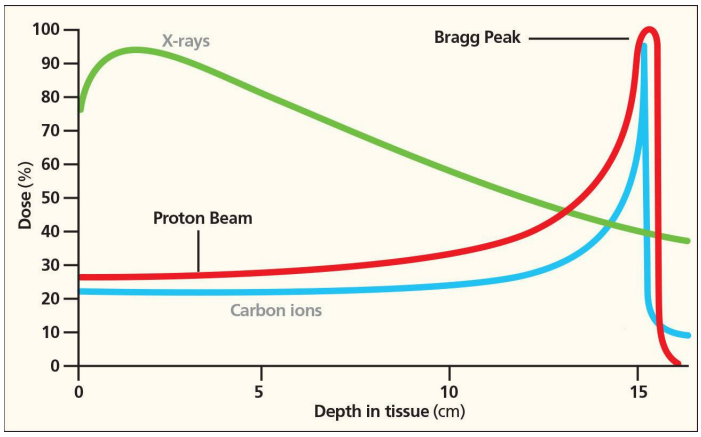

Figure 1.3: A typical Bragg Curve for protons (in red) and for Carbon ions (in blue). In green is reported the energy loss of X-rays in the medium, for take a first comparison between the use of radiotherapy and hadrontherapy for treating cancer.

As it is possible to see in Figure 1.3, in case of X-rays the energy loss is big at the beginning of the medium and then tends to decrease. On the contrary, for charged particles it stays constant at the medium entrance until the Bragg Peak, where protons or carbon ions lose all their energy and are stopped there. The small tail after the Bragg Peak is present for nuclei only and is due to secondary ions produced in fragmentation processes of the impinging carbon ion..

These differences between X-rays and charged particle (and so between radio and hadron-therapy) and the one between the use of protons or carbons are going to be deeper analyzed in the last section of this chapter.

1.2.2 Nuclear fragmentation

The nuclear fragmentation is a non elettromagnetic process that became important at the energies used in hadrontherapy. It is a nuclear collision

between the projectile and the target nuclei, that can be divided in *central collision* (that occurs in a $\sim$ 10% of cases and brought to the complete distruction of the projectile and the target) and in *peripheal collision* (that is more probable and produced a number of secondary products).

In particular, in hadrontherapy the interest is focused on the peripheral collisions, that can occur in four ways:

1. In the case we are using protons as projectile:
    - collision of a proton on a proton does not produce fragmentation;
    - collision of a proton on a nucleus produces the fragmentation of the target nucleus only.
2. In the case we are using ions as projectile:
    - collision on a proton will produce the fragmentation of the projectile only;
    - collision on a nucleus will produce the fragmentation of both, projectile and target.

The main goals of FOOT (**F**ragmentati**O**n **O**f **T**arget) project are the study of two processes: the fragmentation of the target (proton on nucleus) and the projectile fragmentation (ion on proton). One of the problems in the fragments detection is that in peripheral collision the momentum and energy transferred are very small, because the overlap zone is small and only few nucleons interact during the collisions. So, in the case of target fragmentation is very difficult to detect the secondary products, due to their low energy they don't exit from the target. The solution is to approach this problem with the inverse kinematic, but this part is going to be treated deeper in the next chapter.

The fragmentation process can happen in two different steps, reported in Figure 1.4: *abrasion process* and then *ablation* [6]. The first stage involves nucleons, which gained a certain amount of energy and are expelled by the target; and in the same way some nucleons are expelled from the projectile too. In the second stage take place the thermalization and de-excitation of the remaining nuclei with emission of light and intermediate mass fragments. During the abrasion process a fireball is also created, which evaporate during the ablasion [7].

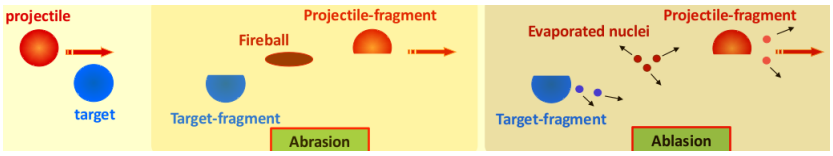

Figure 1.4: Abrasion and Ablation Model in two stages. In this imagine is reported the general case of two nuclei interaction, i.e. a collision of an ion on a nucleus.

1.3 Radiobiological Effects

To understand better the use of the hadrontherapy, it's important to introduce some physic and biologic quantities that characterize the particle therapy.

1.3.1 Physical aspects

Two parameters are of fundamental importance to understand the capability of the hadrontherapy to cure patients:

1. ABSORBED DOSE:

   Radiobiological effects in hadrontherapy (and radiation therapy in general)

are correlated to the absorbed dose, i.e. the mean energy deposited by ionizing radiation (E) per unit mass (m) [8]:

$$D = \frac{\mathrm{d}E}{\mathrm{d}m}$$

The Absorbed dose, as defined, is measured in *Gray (Gy)* in the SI (international system of unit): $1\,\mathrm{Gy} = 1\,\mathrm{J/kg}$ (1 joule of absorbed radiation by 1 kg of mass).

2. LINEAR ENERGY TRANSFER (LET):

   It refers to the transferred energy from a ionizing radiation to a medium per unit distance, so it is linked only to the energy loss of the primary charged particle due to electronic collisions. The higher is the LET value, higher is the transferred energy and more damage the radiation will make to the DNA chains (see next subsection). The LET can be write as:

$$L = \frac{\mathrm{d}E}{\mathrm{d}x}$$

   where $\mathrm{d}E$ is the energy loss of the charged particle due to electronic collisions when transversing a distance $\mathrm{d}x$. The unit of measurement for LET is $\mathrm{KeV}/\mu\mathrm{m}$. For example, protons and photons are *low*-LET while carbon ions are *high*-LET because of their larger ionization density.

Moreover as the Bragg Peak is of the order of few millimeters and tumors are in the order of centimeters, it's necessary to overlap more than one Bragg Peak. This technique is called *Spread Out Bragg Peak (SOBP)*, visible in Figure 1.5 [9].

1.3.2 Biological aspects

To cure a cancer, it is not necessary to kill a cell, but it is enough to prevent its duplication, i.e. damaging its DNA. This is possible in two ways [10]:

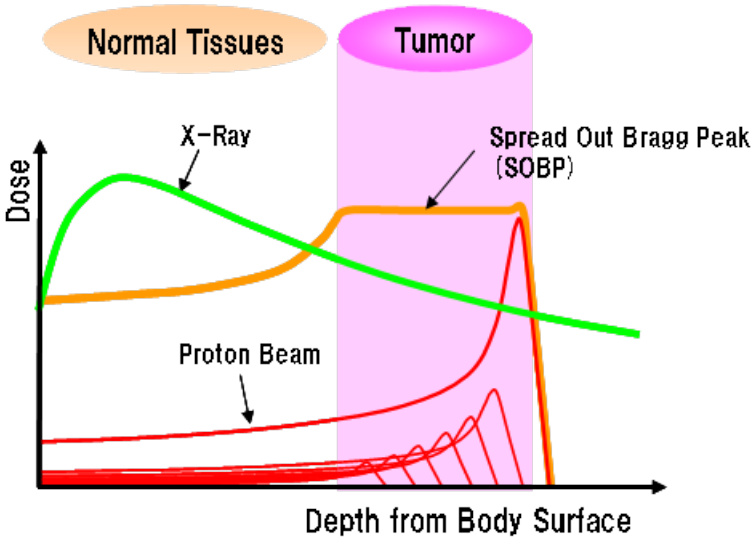

Figure 1.5: The orange line shows the SOBP as the result of the sum of different dose distributions (red lines). The green one is the released dose of X-rays.

- Direct Way: the radiation hits the DNA, damaging its structure (see Figure 1.7, reported below);
- Indirect Way: the radiation hits the water copiously present in the cell, this caused the production of free radicals (very reactive neutral atoms or molecules due to an odd electron) and these radicals attach chemically the DNA chain.

For what concern the indirect way: a radiation that hits on a water molecule may free an electron $H_2O \rightarrow H_2O^+ + e^-$, now the electron may be captured by another water molecule and generate an H_2O^-. Now two reactions can occur:

$$H_2O^- \rightarrow H_o + OH^-$$

$$H_2O^+ \rightarrow H^+ + OH_o$$

Here, the subscript o (as in H_o and OH_o) indicates the free radicals, i.e. an atom or a molecule, that has an unpaired valence electron. These products

may combine in three different ways, assembling two different final molecules:

- WATER MOLECULE: it is the product of two harmless reactions

$$H_o + OH_o \rightarrow H_2O$$

$$H^+ + OH^- \rightarrow H_2O$$

- PEROXIDE OF HYDROGEN: it is created when two OH_0 combine together causing a cell damage for this anomalous production:

$$OH_o + OH_o \rightarrow H_2O_2$$

For what concern the direct way, as we have seen before, an important aspect is the LET which depends on the particle, or better from its charge (as shown in Figure 1.6). Higher charged particles have a less linear trajectory,

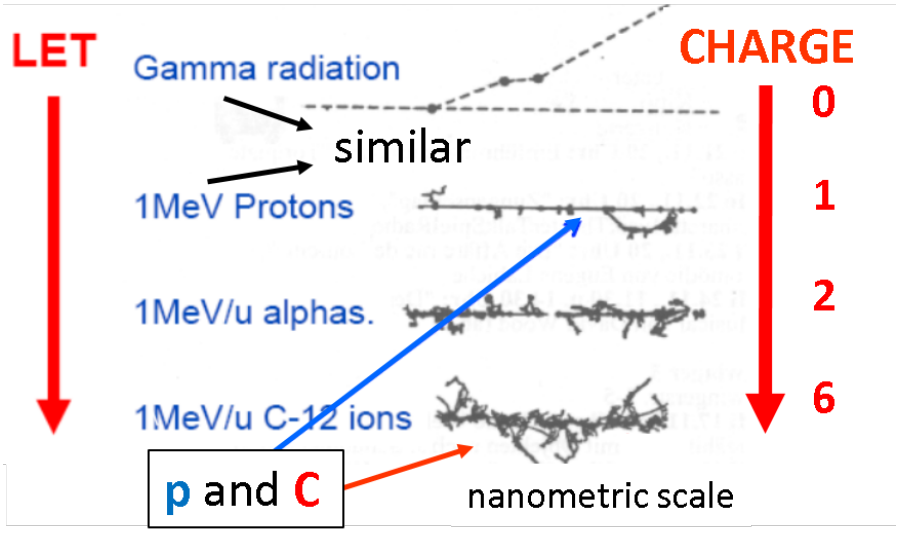

Figure 1.6: Comparison between the ionization density of gammas, protons, alphas and carbon ions. Higher charge correspond to a higher LET and so to a higher DNA damages.

because of their bigger stopping power (-dE/dx). This caused the so called

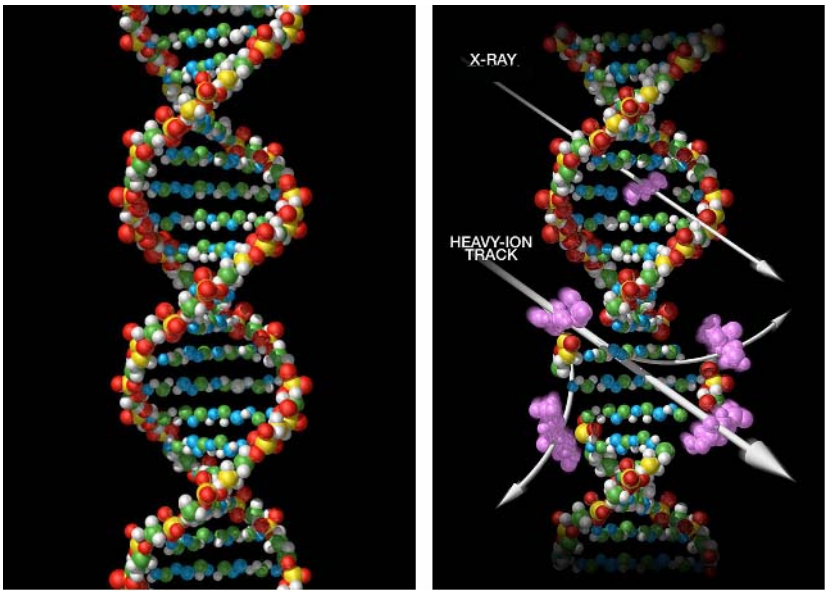

Figure 1.7: DNA damages from photons and heavy-ion, it's shown the bigger damage caused by the second track.

double strand break, which is more difficult to repair by the cell itself and brings with a bigger probability to the cell death, as reported in Figure 1.7.

Two other physical quantities influence the damaging effect of the radiations:

1. RELATIVE BIOLOGICAL EFFECTIVENESS (RBE):

   It is a sort of estimation of the efficacy of the projectile and so it depends on the radiation type and energy, on the dose deposition and the biological system (tissue or cell type). The equation that define the RBE is:

   $$RBE = \frac{D_{ref}}{D_{test}}$$

   It is the ratio of the reference absorbed dose of a standard radiation (D_{ref}, typically the X-rays from ^{60}Co), to the absorbed dose of the radiation under study (D_{test}) that produces the same biological effect. The RBE is an important quantity because it describes the power of

the radiation in killing the tumor cells. For heavy charged particles at the start of their path (high energy), the LET is low and the RBE is about 1 (for protons a typical value is 1.1), while at the end (low energy, in the Bragg Peak zone) the LET is high and so is the RBE. This means that ions are more effective than photons in killing tumor cells.

2. OXYGEN ENHANCEMENT RATIO (OER):
   As mentioned before, the presence of oxygen brings a higher probability in the free radicals production. In a tumor, like for every cell in a human body, the oxygen is brought by blood vessels, but not always this happens in a cancer. If vessels are not generated faster enough or do not work well, hypoxic regions can develop in the tumor, i.e. regions where the oxygen did not arrive to the tumor. These are often localized deep inside the cancer and caused a great reduction of the radio-sensitivity of cells. This problem is described by the OER parameter, which is defined as the ratio between the necessary dose for hypoxic region and for the well oxygenated ones:

$$OER = \frac{D_{hypoxic}}{D_{not-hypoxic}}$$

   These values can stand between one (well oxygenated tumor) to three (strongly hypoxic tumor). As it's possible to see in Figure 1.8, for having the same survival fraction, the hypoxic tumor needs to receive a higher dose in gray. Radiations with *high*-LET usually have a lower OER and this can be used for increasing the power of radiation treatment.

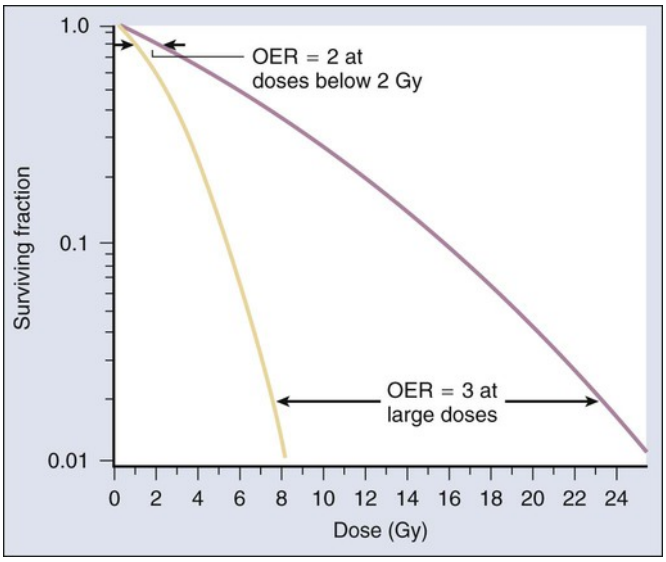

Figure 1.8: In purple the curve for hypoxic cells and in orange the one for aerobic cells. As it's possible to see, the ratio at the same survival level is the OER: bigger is the difference in the curve trend, bigger is the ratio.

1.4 Comparisons

In this section some recaps and comparisons are reported to show the pros and cons for hadrontherapy in respect to the radiotherapy and between the use of protons or ions, in particular, then, the case of using ^{16}O for the hypoxic tumors.

1.4.1 Hadrontherapy and radiotherapy

In radiotherapy, photons beams are used and as was shown in Figure 1.3 (the green line) their energy loss decrease with the deep of their path. This causes a radiation release of the same size order in the tumor and in the healthy cells before and after the tumor itself. The first step in this direction is the IMRT (Intensity Modulated Radiation Therapy), i.e. the overlap of different photons beams from different directions. This allow a higher dose

in the tumor keeping constant the dose in the normal cells, which remain constant but still not low enough for being sure to prevent other damages.

Hadrons beams, instead, have a completely different trend for what concern the energy loss in a medium: a low release of energy before the Bragg Peak and the peak itself, where the particle lose almost its whole energy. This allow to keep low the radiation to the healthy tissue cells and high the radiation in the cancer, always using (as mentioned in the previous section) the Spread Out Bragg Peak (SOBP) for covering the whole area of the tumor.

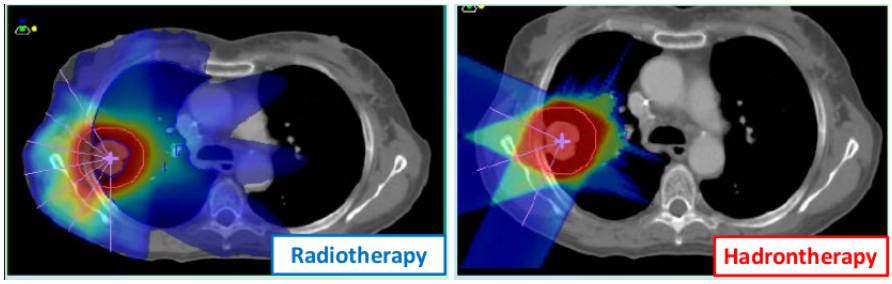

Figure 1.9: A comparison between the radio (at left) and the hadron-therapy (at right). In blue the areas with less energy loss and in red the high-LET regions, where the tumor has to be placed. The radiotherapy dose arrives till the healthy tissues (in this case the hearth) while the hadrontherapy preserves them better.

An important effect that must be considered is the, before mentioned, multiple Coulomb scattering. This process makes the beam wider and so causes a dose release in a bigger area, which can be outside the tumor too. The probability of this scattering becomes lower for particles with a bigger mass (that makes ions a better candidates with respect to protons). Another process that can happen at the energy of hadrontherapy (about 200 MeV/u) is the nuclear fragmentation (exposed in subsection 1.2.2), the fragment produced must be considered in the planning of the treatment. So these contributions have to be studied and that's the first reason of the

FOOT experiment.

The bigger disadvantage of hadrontherapy is the cost of cyclotrons and syncrotrons and the space they need (Figure 1.10). Infact, a IMRT treatment costs about $10,000$ euros, while for the hadrontherapy the cost is almost millions of euros.

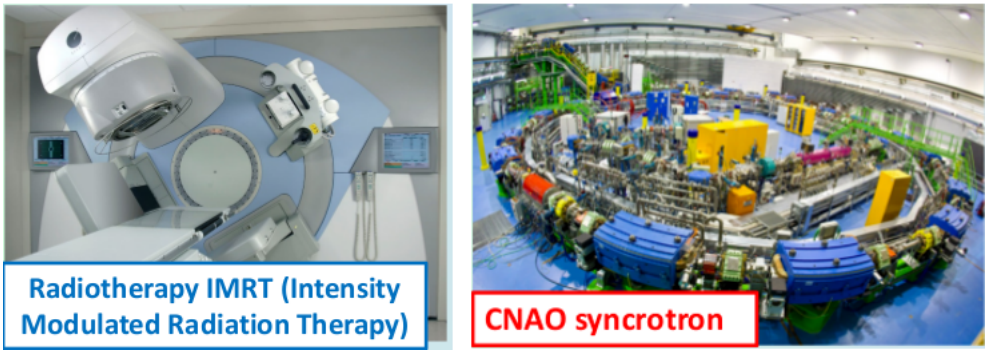

Figure 1.10: At right a facility for hadrontherapy and at left for radiotherapy.

1.4.2 Protons and ions

For what concern the use of protons beams or carbon-ions beams, there are some considerations that have to keep in account:

- At first, the dose from protons is lower than the one released from heavy ions (RBE almost 1 at start and 3-4 at the Bragg Peak);
- The disadvantage of ^{12}C is the "tail" (Figure 1.11) that they present after the Bragg Peak, which is caused by the products of nuclear fragmentation. For what concern the ions heavier than Carbon, they are difficult to use because they produce more fragmentation and have a higher LET in the first zone before the Bragg Peak, causing a higher damage to the healthy tissue;

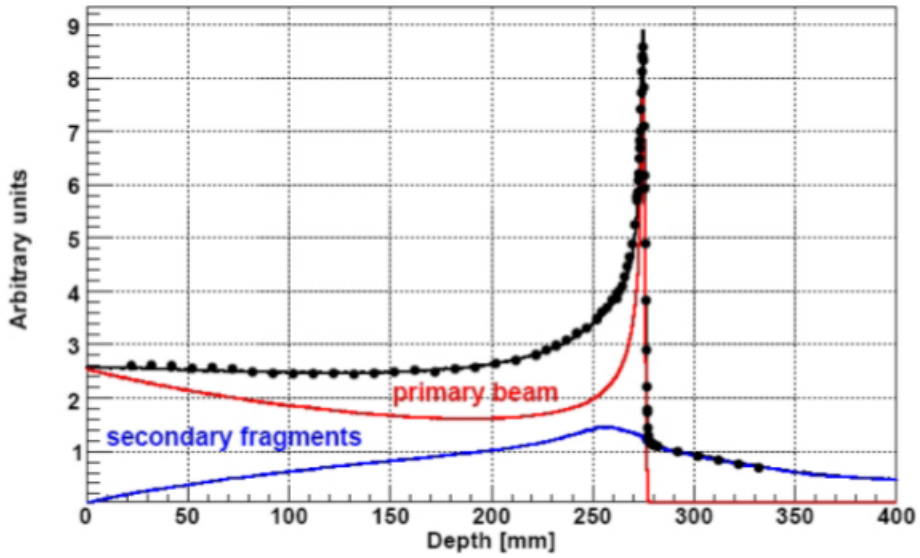

Figure 1.11: Bragg curve for a ^{12}C beam with kinetic energy of 187 MeV/u, they present a tail caused by the fragmentation.

- Carbon-ions present a minor diffusion and a less probable Coulomb scattering, and so are more precise in hitting the tumor cells only [11].

Moreover, oxygen beams are increasingly considered as a fundamental tool against hypoxic tumors. Since it has been shown that OER decreases substantially with LET, the reason for using oxygen beams is basically driven by their similar characteristics as compared to carbon, but with an importantly larger LET distribution, able in contrasting hypoxia (lack of cell oxygenation). However, in normal (aerobic) conditions, the larger fragmentation of oxigen-ions beam in the target and entrance channel, makes their use less convenient as compared to lower Z ions (such as C). The challenge in an assessment considering a possible use of Oxygen is then a trade-off between the LET advantage and the worse fragmentation in the normal tissue, which should be evaluated, case by case, accordingly to geometry, tissue sensitivity and other patient based characteristics. In most of the cases, oxygen beam

is envisaged not as a full alternative option, rather as a boost in combination with other types of (lower LET) particles.

After the evaluation of all the processes that are related to hadrontherapy and their pros and cons, the FOOT project is going to study better the fragmentation of target, where there is a lack of data, both for proton and ion beams. In addition, the project will provide also projectile fragment production cross sections for new, high LET ions, like oxygen beams and will cover the energy gap in available data of ^{12}C ion fragmentation cross sections.

These studies are very important for developing a new generation of biologically oriented Treatment Planning Systems for proton and ion therapy. All the physics, motivations and experimental setup for FOOT project is going to be shown in the next chapter.

Chapter 2

The FOOT Project

The FOOT (**F**ragmentati**O**n **O**f **T**arget) experiment has been conceived in order to perform a set of measurements of nuclear fragmentation cross sections which will be used to develop a new generation of biologically oriented Treatment Planning Systems for proton and ion therapy. This because in the energy range of therapeutic application (50-250 MeV for protons and 50-400 MeV/u for carbon ions), the fragmentation process has not been completely covered by experimental measurements.

Furthermore, the products of the target fragmentation could be one of the causes for the increasing of the proton RBE, that is estimated to be 1.1. This constant value may be an underestimation of the real dose released in the healthy tissues and this leads to a difficulty in the Treatment Planning System (TPS), that, for this reason, has not a standard protocol for hadrontherapy.

In the case of proton therapy, only the fragmentation of the target may occur, that produces low energy fragments with short range, these particles have a short range, very high LET and so very high RBE. This process may have an impact on the channel entrance of protons and it's crucial to measure the consequences on the human body.

In the next sections motivations of the FOOT experiment are going to be seen in details and then some experimental issues will be treated, with a recap about the detectors setup.

2.1 Motivations of the Experiment

For what concerns the Hadrontherapy, the first aim of FOOT is the measurement of target fragment production cross sections for proton beams. In addiction, FOOT will provide also projectile cross sections for high LET ions, as carbon and oxygen, and will cover the leak of measurements in the energy range of the hadrontherapy.

The Treatment Planning System needs an accurate knowledge of the released dose and consequently of the possible biologic effects; this makes the study of the nuclear fragmentation at the energies of the hadrontherapy necessary. Each fragment contribution interacts with the cells producing a different damaging result, meaning that the damages depend on the type of beam and its energy.

Then in the case of proton therapy the target fragmentation is more relevant in the entrance region, where the proton energy is still quite large with respect to the peak region where ionization is more probably than fragmentation. Now, since the targets fragment are reduced at very low energies, the particles are going to travel a distance of few microns, and so this makes their experimental detection difficult. For this reason, FOOT is going to use an inverse kinematic approach (described in the next section).

In the case of direct kinematic approach, instead, FOOT is useful to measure the projectile fragmentation for each type of beam as carbon, oxygen and helium.

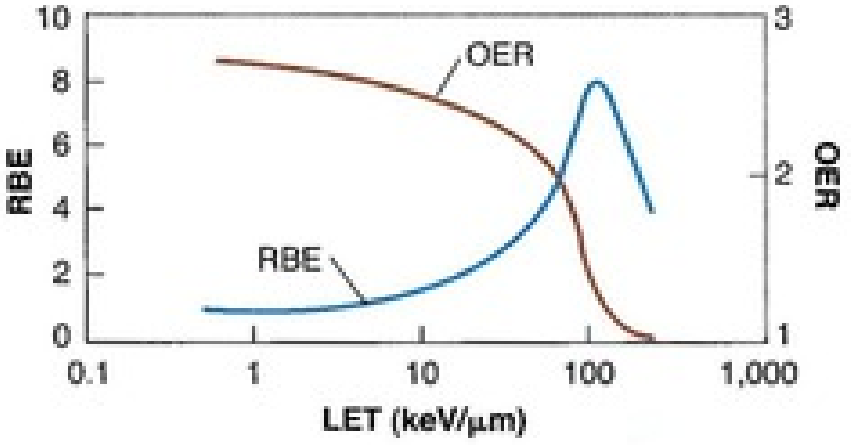

Figure 2.1: In this graph is reported the relationship between OER and LET, and between RBE and LET.

1. CARBON:

   Carbon-ions present a minor diffusion and a less probable Coulomb scattering than protons, and they have also a higher released dose in the Bragg Peak. The disadvantage of Carbon is the "tail" that they present after the Bragg Peak, which is caused by the products of nuclear fragmentation.

2. OXYGEN:

   Oxygen beams are considered a fundamental tool against hypoxic tumors, because due to the low OER value in corresponding to high LET, especially beyond $\sim$ 100 KeV/μm (Figure 2.1), so the reason to use oxygen ions is the high-LET able to be effective in contrasting hypoxia[1]. However in aerobic conditions, their larger fragmentation in the target makes the use of oxygen not convenient in respect with lower

[1]Hypoxia is a condition in which the body or a region of the body is deprived of adequate oxygen supply at the tissue level. Hipoxia in a tumor causes a lower probability in the free radicals production (as described in Subsection 1.3.2)

Z ions (as carbon). As a matter of facts, oxygen is used as a boost in combination with other types of particles.

3. HELIUM:

   Helium beams are considered a possible alternative to protons, because of their lower multiple Coulomb scattering, allowing an higher resolution in lateral spread (see Figure 2.2). Then, Helium is convenient above Carbon for the lower cost but also for the lower impact of nuclear fragmentation, especially in the tail after the peak

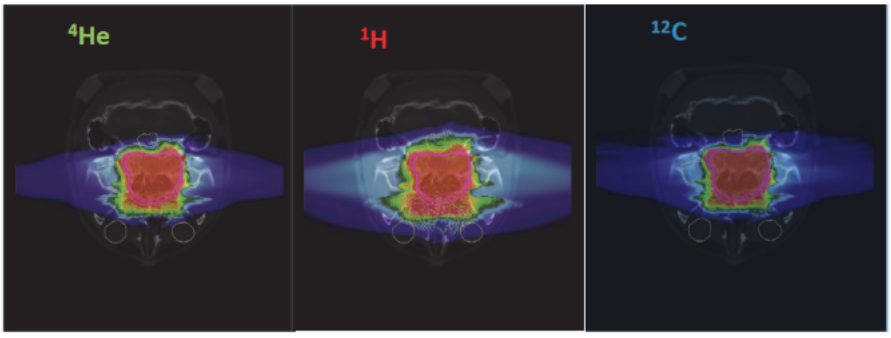

Figure 2.2: Comparison of treatment plans on a skull chordoma: Helium (^{4}He) is more convenient as compared to protons in the case of lateral organs at risk.

Another application of the FOOT project is the radioprotection in space, i.e. studying the risk assessment for astronauts in view of long duration space missions. Infact, there is a common ground between protecting astronauts from the harmful effects of space radiation (as the energetic particles product by Solar Particle Events, Galactic Cosmic Rays, etc.) and providing tumor therapy. The overlap is in terms of energy: the energy for tumor therapy is not so far from the energy region of the solar flare protons as well as near the peak of the Galactic Cosmic Rays spectrum [12].

2.2 Experimental Strategies for Measurements

The study the projectile fragmentation, do not present particular problems because the produced fragments have enough energy to escape the target and to travel all the detector, allowing a traditional approach of direct kinematic.

While to perform measurements on the target fragmentation consequently to a proton beam, the main obstacle is the short range of the produced fragments. In Table 2.1 it's shown the range of the fragments produced by incident protons of 180 MeV in a water target; the range is of the order of tens of μm that prevent the fragments to escape the target.

Fragment	**E(MeV)**	**LET(MeV/μm)**	**Range(μm)**
^{15}O	1.0	983	2.3
^{15}N	1.0	925	2.5
^{14}N	2.0	1137	3.6
^{13}C	3.0	951	5.4
^{12}C	3.8	912	6.2
^{11}C	4.6	878	7.0
^{10}B	5.4	643	9.9
^{8}Be	6.4	400	15.7
^{6}Li	6.8	215	26.7
^{4}He	6.0	77	48.5
^{3}He	4.7	89	38.8
^{2}H	2.5	14	68.9

Table 2.1: Expected average physical parameters for target fragments produced in water by a 180 MeV proton beam. The initial average energies of secondary fragments are calculated according to the Goldhaber formula [13].

The Range is calculated from the energy of the fragment, which is derived from the Goldhaber formula [13]:

$$E_{frag} = \frac{3}{5}\left[\frac{M_{target} - M_{frag}}{M_{target} - 1}\right]\frac{p_F^2}{2m_p} \quad \text{where} \quad p_F = 281\left(1 - M_{frag}^{-0.568}\right)$$

Here, p_F is the Fermi momentum, m_p the mass of proton at rest, M_{target} is the mass of the target and M_{frag} the mass of the fragment.

Now, given a fragment produced by a proton projectile somewhere in the target matter, the ion can cross and leave the target only if it has been produced at a distance less than few micrometers from the exit surface of the target material. Otherwise the fragment deposits all its energy locally, being trapped inside the target, not allowing any possibilities of detection.

The problem could be solved using a very thin target, but this kind of target provide a lot of issues: it's difficult to be created and the rate of fragmentation is lower and suppressed.

2.2.1 The inverse kinematic approach

To overcome the issues related to the measurements of the target fragmentation, the FOOT approach is to use the inverse kinematic. So, while the direct fragments production reaction is represented by a proton that collides inelastically with the target nuclei (as similar as possible to human bodies nuclei) at rest: the inverse kinematic approach switch the role of the incident proton with the target nuclei. Thus the particle beam is composed of ^{16}O and ^{12}C ions, which are the principal component of the human body, impinging on a proton target, at rest.

By studying the inverse interaction and measuring the four-momentum of the produced fragments and of the incident beam, it is possible to gain experimental access to the inverse decay chain information, performing a

Lorentz transformation. In this way it is possible to take measurements with a thicker ($> \mu$m) target providing a higher fragmentation rate and significant amount of data, without the issues related to the direct kinematic approach.

The problem now stays in the proton target, because the use of a pure gaseous hydrogen target leads to some considerable technical difficulties: its low density and the issues about transport. For these reasons, it has been decided to adopt a double target made of polyethylene (C_2H_4) and graphite (C), which are easier to produce and manage; the cross section measurement of the only hydrogen target can be obtain performing a subtraction of the measured cross sections in both target:

$$\sigma(H) = \frac{\sigma(C_2H_4) - 2\sigma(C)}{4}$$

The subtracting cross section method, with a CH_2 target instead of C_2H_4, has already been tested at Ganil (France) with the results shown in Fig. 2.3 [14].

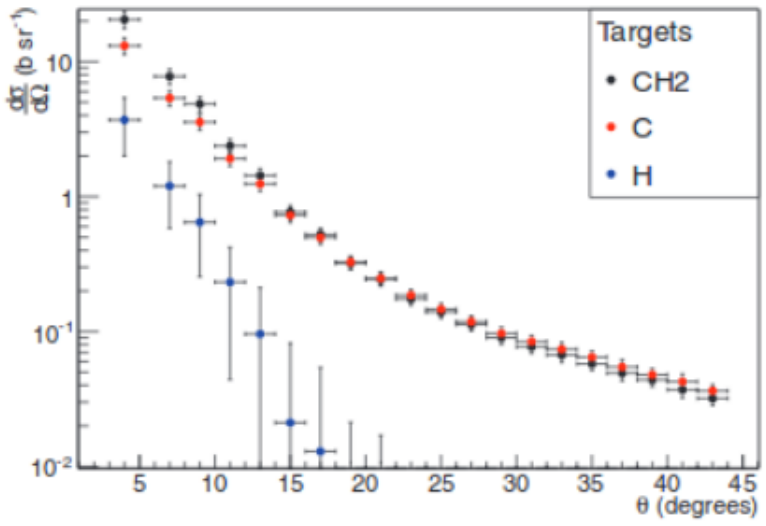

Figure 2.3: Combination of carbon and CH_2 targets angular distribution to determine the hydrogen one for ^{2}He fragments. The angular distribution for the hydrogen target is the difference between both, divided by two.

2.2.2 Two different setups

To introduce a new proton RBE model, which includes the effects of nuclear interactions, the FOOT experiment has to accomplish different requirements regarding the identification of the nuclear fragment particles created by the incident protons. Both heavy and light fragments have to be detected and studied.

Due to the mass difference of the produced fragments, the heavier ones (typically with $Z > 3$) are mainly produced in the forward direction (within $\theta \leq 10^o$), while the lighter ones at larger angles (as it is possible to notice in Fig.2.4). Due to this difference, it has been decided to adopt two different setup in order to focus the attention on the two species of fragments. The

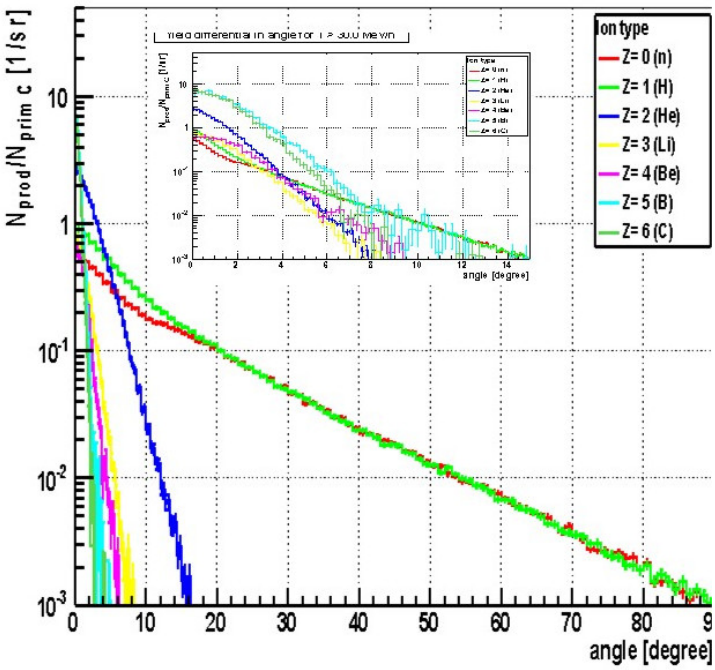

Figure 2.4: Angular distribution for the emitted fragments: the lighter nuclei are emitted until 80^o while the heavier ones (with $Z > 3$) stay in the limit of 10^o.

first setup focuses on the fragments with $Z > 3$, while the experimental ar-

rangement designed to detect the lighter fragments is based on the Emulsion Cloud Chamber (ECC) and it will be described in Subsection 2.3.2.

2.3 FOOT Detector Setup

To measure the fragment production due to protons and heavy ions, it is necessary to use beams of carbon and oxygen ions with energies about 100-300 MeV/u, and so CNAO (Centro Nazionale di Adroterapia Oncologica, Pavia, Italy), HIT (Heidelberg Ion-Beam Therapy Center, Heidelberg, Germany) and GSI (Gesellschaft für Schwerionenforschung, Darmstadt, Germany) hadrontherapy centers are chosen to be the three most suitable locations for the experiment, because they are equipped with carbon and proton beams with energy and resolution typical of the hadrontherapy treatment. Considering the dimensions of the available experimental rooms, all the detectors have to be allocated in an approximatively 2 meter length along the beam line. Thus both the experimental setups (to detect low and high Z fragments) have been designed in order to be easily movable ("table top setup") fitting the space limitations and covering the fragments angular spread [12].

One of the main requirement of the FOOT detector design is the identification of the fragments measuring their momentum, kinetic energy, time of flight (TOF) and the energy loss ($\mathrm{d}E/\mathrm{d}x$). The momentum, kinetic energy and total energy can be obtained by following relations:

$$p = mc\beta\gamma \qquad E_k = mc^2(\gamma - 1) \qquad E_k = \sqrt{p^2c^2 + m^2c^4} - mc^2$$

where $\beta = v/c$ and $\gamma = 1/\sqrt{1-\beta^2}$ are derived from the fragment TOF. The mass of the produced fragments can be extracted by using contemporary two of the previous formula; in this way the mass can be obtained in three different ways correlated between them.

2.3.1 Heavy nuclei detection

In the first experimental setup the main interest is focused on the fragments with $Z > 3$, whose cross section data are missing in the literature. A schematic view of the detector is shown in Figure 2.5.

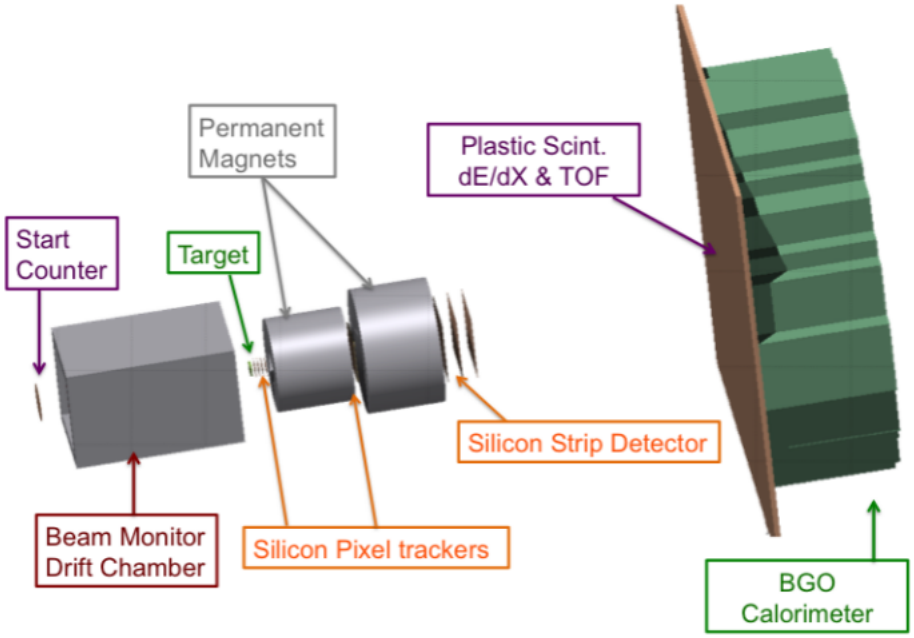

Figure 2.5: Schematic view of the FOOT apparatus for the detection of heavy fragments [12].

The FOOT apparatus for the detection of heavy fragments can be divided in three regions:

1. PRE-TARGET AND TARGET REGION: this first region contains:

   - The Start Counter (SC): a thin plastic scintillator detector (250 μm of thickness with 4 channels read out by fast PMTs) used to provide trigger information and the start of the TOF.
   - The Beam Monitor (BM): a drift chamber (21 cm x 11 cm x

11 cm), composed of six planes of alternated horizontal and vertical wire layers. Each layer has three cells to provide the measurements in terms of the drift coordinates. The purpose of the BM is to measure the beam direction (necessary for the inverse kinematic approach) and reject the events in which the primary ion has fragmented before the target.

- The Target: both polyethylene and graphite targets are needed to adopt the subtraction of cross section method. The thickness of the target is chosen to be about 2 mm, avoiding both the fragment trapping effect and the decrease of the nuclear interaction rate.

2. THE MAGNETIC SPECTROMETER: which is formed by:

- The Front Silicon Pixel Tracker (FSPT): four layers of silicon detector placed just after the target to be used as vertex detector.
- The Magnets: two permanent magnets with Halbach geometry[2] (Figure 2.6) to perform the momentum measurements.
- The Rear Silicon Pixel Tracker (RSPT): two layers of silicon detector, designed as an enlarged copy of the Front Silicon Pixel Tracker.
- A Micro Strip Detector (MSD): a silicon strip detector of 9x9 cm^2 of transverse dimension composed by 3 layers each one composed by two orthogonal silicon strip layer of 70 μm thick, each for the $xy-$reconstruction.

[2]A Halbach cylinder is a special arrangement of permanent magnets that produced a magnetic field confined entirely within the cylinder with low field outside.

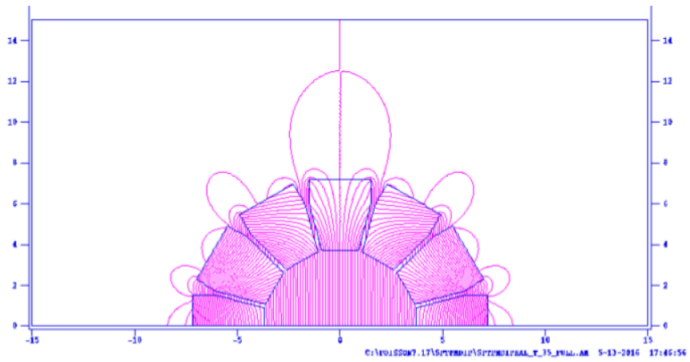

Figure 2.6: Calculated magnetic field map for the design of the FOOT Permanent Magnet in Halbach geometry [12].

3. THE CALORIMETER REGION: downstream the magnetic spectrometer the fragments travel $\sim$ 1 meter to reach the ΔE and TOF detector:

   - Scintillator (SCI): $22 + 22$ plastic scintillator bars arranged in two orthogonal layers, each bar is 20 cm long and 3 mm thick. Goal of the scintillator is the measure of the energy deposited ($\mathrm{d}E/\mathrm{d}x$), the stop of the time of flight and an estimation of the fragment position. The total time resolution is $\sim$ 70 ps and the energy resolution is estimated to be between 3% and 5%.
   - Calorimeter (CAL): a cylindrical detector with 20 cm radius, formed by 360 elements of BGO crystals ($Bi_4Ge_3O_{12}$) of 21 cm thick and with a density of 7.13 g/cm^3.

2.3.2 Light nuclei detection

The experimental apparatus designed to detect light fragments is based on the Emulsion Cloud Chamber (ECC). The start counter and the beam monitor are the same as the first experimental setup, as they provide information about the incident particle beam, while the other detectors are replaced

by the ECC. The ECC is composed by a sequence of nuclear emulsion films

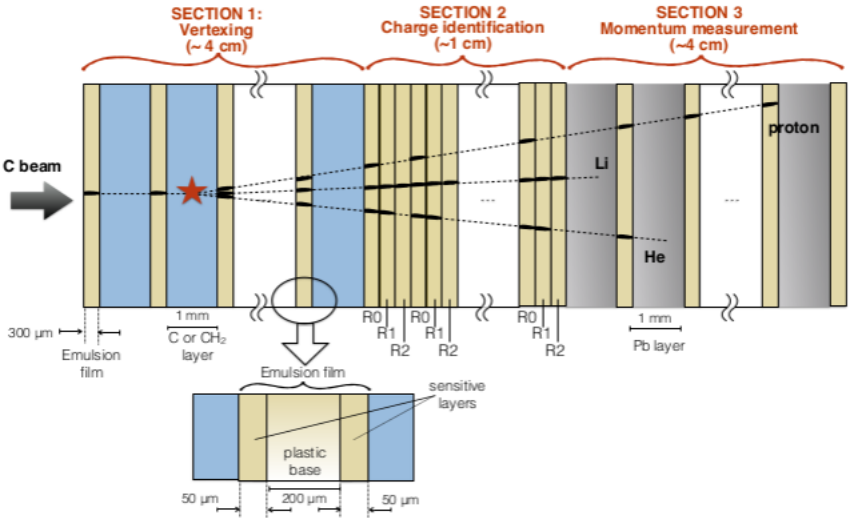

Figure 2.7: Schematic view of the FOOT apparatus for the detection of light fragments [12].

(detector) interleaved with passive material of C and CH_2 (target) and Pb. The passage of a charged particle in the nuclear emulsions produces an image, turned into a sequence of silver grains which are lied along the trajectory of the particle with a density almost proportional to the energy loss [15]. The structure of ECC (Figure 2.7) proposed for the FOOT experiment consists of three different sections:

1. TARGET AND VERTEXING: it is about 4 cm and it is formed by 60 alternated layers of emulsion films (300 μm) and target layers (1 mm of C/CH_2), operating as vertex detector with the purpose to track all the charged particles.

2. CHARGE IDENTIFICATION: this section is $\sim$ 1 cm of thickness and it is composed of emulsion films only, with the aim of identifying the atomic numbers of low charged fragments (proton, helium and lithium).

3. MOMENTUM MEASUREMENT: the thickness is $\sim$ 4 cm and it is composed by 10-50 alternated layers of emulsion films (300 μm) and absorber layers (1 mm of Pb), adopted to measure the fragments range in order to estimate the particles momenta. The number of layers varies according to the incident beam energy.

Chapter 3

Fragmentation Cross Sections

The study of the nuclear fragmentation process is relevant for many fields of interest, from the hadrontherapy, to the spatial vehicles shielding design, to work safely in space with acceptable risks from galactic cosmic ray. Indeed, the measure of the fragmentation cross section is an important information to estimate how this process modifies dose distributions and biological effectiveness in oncological therapies with ion beams.

At the moment, simulations are used to deal with these problems. Such approach presents a considerable uncertainty, both on the fragmentation cross sections and on the different radiation biological effectiveness. Due to the reduced number of measurements in the interested energy ranges, therefore a larger amount of fragmentation cross section data is necessary: a wide energy range and different ions and materials have to be explored. For targets, the best ones to simulate soft biological tissues are plastics and water, because the human body mostly consists of four elements: hydrogen, carbon, oxygen and nitrogen.

One of the most important aspects in this research field is to understand and to characterize physics and radiobiological effects like biological damages

related to ion fragmentation [16]. In fact, nuclear fragmentation of the projectile nuclei may deposit undesired energy in healthy tissues surrounding and beyond the target. This is a less significant phenomenon in the proton therapy, even if neutrons arising from nuclear reactions may travel and deliver dose far from the irradiation region.

In some cases, nuclear reactions can actually be profitably exploited, for example, the production of the unstable fragments, decaying through the β^+ process, can be used for quality assurance of the beam delivery. The positron from the β^+ decay is quickly stopped and annihilates, producing two peculiar back-to-back gamma rays that can be detected and traced up to the annihilation vertex [17]. However, neutrons are neutral particles, with a lower interaction rate with respect to the charged ones. For this reason, they can deliver doses to distant tissues, possibly causing late secondary tumors [18].

3.1 Cross Sections Measurement

The measurement of the cross section may be performed in different ways [19]:

1. INCLUSIVE CROSS SECTION

   The inclusive cross section is defined as the cross section of a process in which only a subgroup of final state particles are specified. An inclusive reaction is typically denoted as $P + T \rightarrow F + X$, where the projectile P and the target T make up the initial state. The final state consists of the measured projectile fragment F and the outgoing particles X, which may or may not be measured.

2. EXCLUSIVE CROSS SECTION

   An exclusive cross section results when all outgoing particles are assumed to be detected. This kind of experimental measurement is more difficult than the previous one, because all outgoing particles have to be measured and identified.

In literature, it is possible to find different cross section measurements for different nuclear reactions, so it is helpful to briefly define them.

The **charge changing cross section** (denoted by $\sigma_{\Delta Z \geq 1}$) is defined as the cross section of a process in which a charge difference of at least one is present between the projectile and the fragment. Whereas, the **mass changing cross section** ($\sigma_{\Delta A \geq 1}$) is defined to be the cross section for removing at least one nucleon from the projectile. In Fig.3.1 are reported data collected in this field of study about charge changing cross section, in different ranges of energy and for different combinations of targets and projectiles.

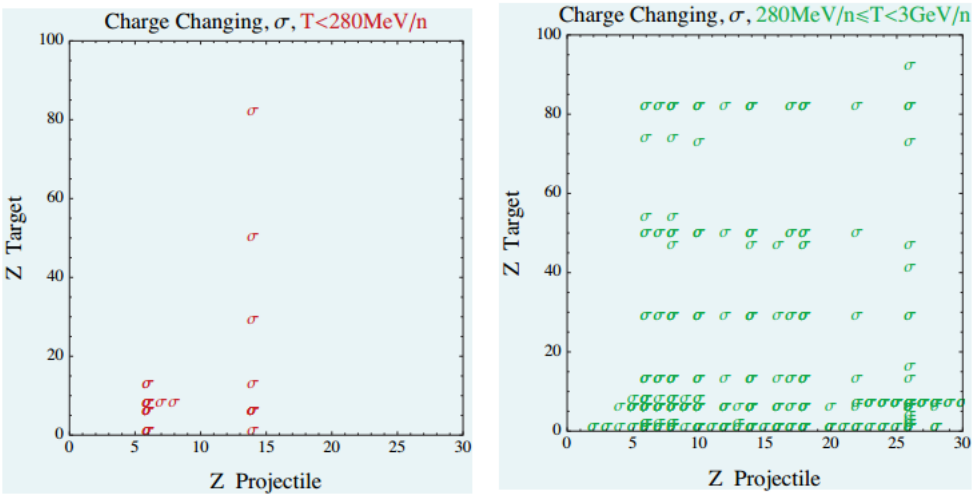

Figure 3.1: The availability of a charge changing cross section measurement for couples of projectiles and targets is marked with a σ for two different kinetic energy ranges: left, the data for T<280 MeV/n and at right, the energy range 280 MeV/n $\leq$ T $<$ 3 GeV/n [19].

Many measurements have been performed, but it is straightforward to notice the lack of data in certain ranges (280MeV/n $\leq$ T $<$ 3 GeV/n and T$<$280 MeV/n), in particular in the region $Z_{projectile} < 10$ and $Z_{target} < 10$, which is relevant for Carbon or Oxigen ion therapy.

The **isotopic cross section** describes the production of a fragment with a given charge and mass. Compared to charge changing cross sections, isotopic cross sections are more difficult to measure experimentally, because each isotope needs to be identified separately. Collected data about isotopic cross section are reported in Fig.3.2. Also in this case, the measurements have been performed in different energy ranges and for different combination of target and projectile. Moreover, the same problem of the lack of measurements is shown in these plots, even more accentuated.

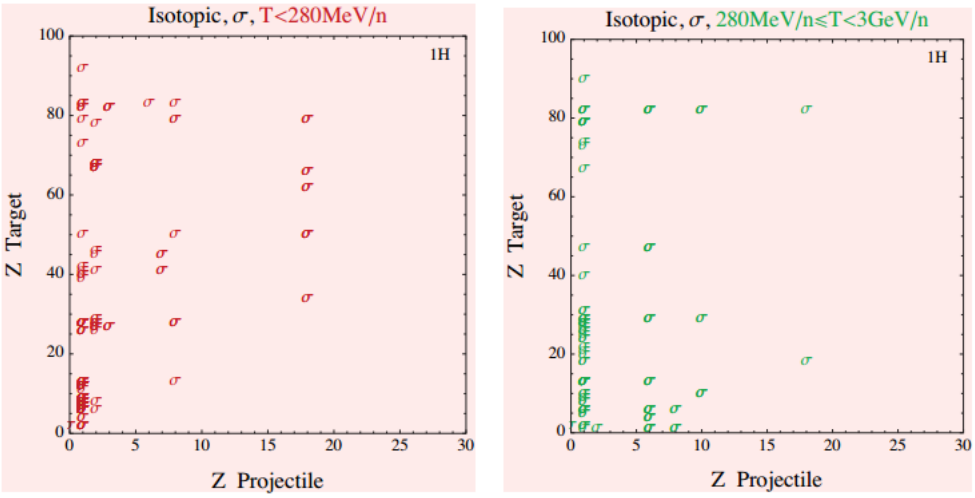

Figure 3.2: The availability of isotopic cross section for the production of a proton (^{1}H fragment) is marked with a σ for two different kinetic energy ranges: left, the data for T$<$280 MeV/n and at right, the energy range 280 MeV/n $\leq$ T $<$ 3 GeV/n [19].

The goal of the FOOT experiment points to the measurement of two more important cross section, in the hadrontherapy field: the **fragment production cross sections** ($\sigma(Z_F)$), that quantify the probability for production of fragments with a given charge; and the **differential cross sections**, which take account angular or energy information, in its calculation. The first is more difficult to measure than charge changing cross section because of the difficulty of identify fragments against the background of projectile particles. The second type of cross section is useful because angular and momentum distribution data can be used to differentiate between models and to estimate two and three dimensional dose distributions into materials. The differential cross section is measured as a function of one or more variables (such as fragment energy E, momentum p, or emission angle θ). For example, a *single* differential cross section may depend only from the angular distribution ($\mathrm{d}\sigma/\mathrm{d}\Omega$), while the *double* differential cross section ($\mathrm{d}\sigma/\mathrm{d}\Omega\mathrm{d}E$) is measured as a function of both the fragment energy (or momentum) and angle: they provide more detailed information on dose distributions than simple angular distributions integrated over all fragment energies or energy spectra taken at a single angle.

In Figs.3.3, 3.4, 3.5 all the fragmentation cross section and the differential cross section measurements have been shown, for different energy ranges and target-projectile combination. In this case, more than in the previous one, the extremely low number of overall measurements and in particular in the hadrontherapy region ($Z_{projectile} < 10$ and $Z_{target} < 10$) is striking and the urgency of covering this deficiency is clear.

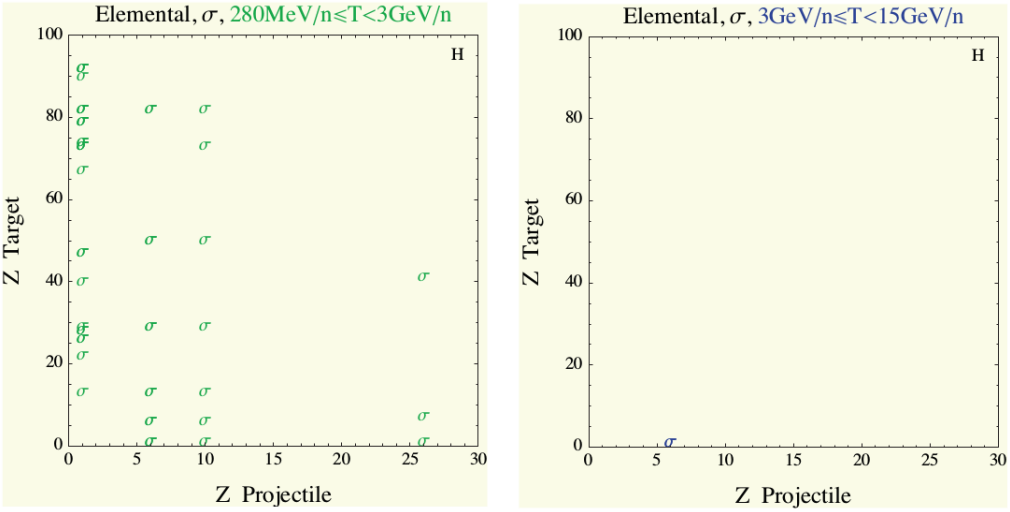

Figure 3.3: The availability of fragmentation cross section for H fragments is marked with a σ for two different energy ranges. Left, the data for a beam kinetic energy of 280 MeV/n $\leq$ T $<$ 3 GeV/n and right, the energy range 3 GeV/n $\leq$ T $<$ 15 GeV/n [19].

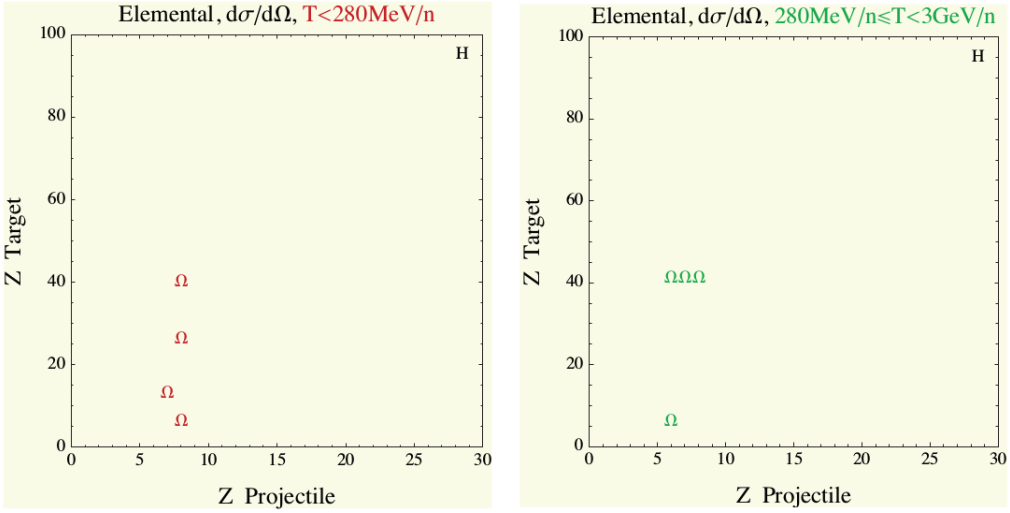

Figure 3.4: The availability of single differential cross section for H fragments is marked with a Σ for two different energy ranges. Left, the data for a beam kinetic energy smaller than 280 MeV/n and right, the energy range 280 MeV/n $\leq$ T $<$ 3 GeV/n [19].

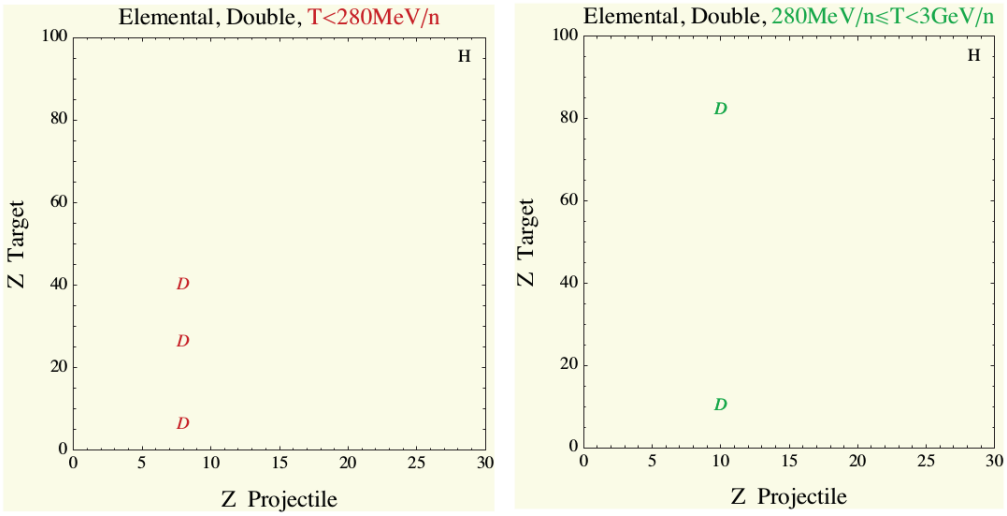

Figure 3.5: The availability of double differential cross section for H fragments is marked with a *D* for two different energy ranges. Left, the data for a beam kinetic energy smaller than 280 MeV/n and right, the energy range 280 MeV/n $\leq$ T $<$ 3 GeV/n [19].

3.2 Previous Data on Fragmentation

A fragment is defined as a charged nuclear particle with a mass and charge that are different from the primary beam particle.

The enhanced relative biological effectiveness (RBE, as defined in subsection 1.3.2) of heavy ions (like carbons), with respect to protons, is one of the main reasons, together with their good ballistic properties, for their use in hadrontherapy. Moreover the RBE increases towards the end of the ion range in the biological material as the energy decreases, thus further improving the already better ion depth-dose distribution (an example for protons is reported in Fig.3.6).

The Continuous Slowing Down Approximation (CSDA) range is a very close to the average path length traveled by a charged particle as it slows down to rest. In this approximation, the rate of energy loss at every point

along the track is assumed to be equal to the total stopping power ($\mathrm{d}E/\mathrm{d}x$). The straggling depends on the fact that the energy loss is not a continuous phenomenon, but statistical. Indeed, two identical particles with the same initial energy will not suffer the same number of collisions and hence the same energy loss. For this reason, the range is modified to consider this statistical distribution of different ranges centered on a mean value.

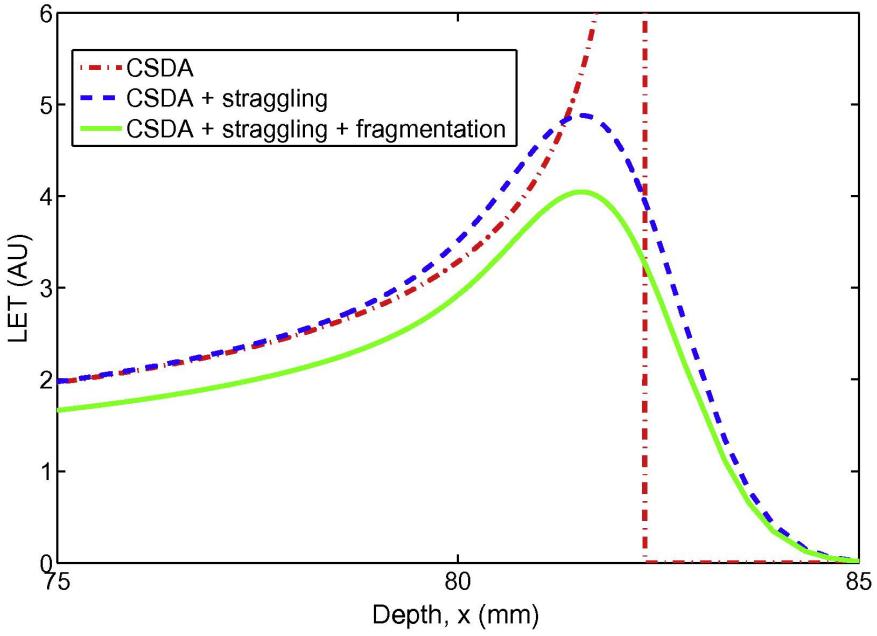

Figure 3.6: Depth-dose distribution of protons in water for kinetic energy $E = 100$ MeV, considering the CSDA (Continuous Slowing Down Approximation, only the stopping power is taken in account) range and adding straggling (depends on the statistic of the energy loss) and nuclear fragmentation.

For example, when Carbon beam proceeds through the matter, it fragments in smaller particles with velocity similar to those of the beam, producing a "tail" in the dose distributions after the Bragg peak and implying the irradiation of the immediately downstream healthy tissues.

In the last years, the studies has been focused on Carbon ion beams, but the abundance and energy spectrum of secondary particles emitted by hadrontherapy beams at larger angles with respect to the primary beam direction are mainly unknown, and, as a consequence, very poorly reproduced by the nuclear model implemented in the Monte Carlo (MC) simulation used to prepare Carbon ion treatment planning systems.

The reliability of the MC estimations can be assessed only by comparing the results of different models with experimental data and, at the moment, the amount of data on fragment energy distribution at large angles is rather poor [20].

There are more than one model to simulate nuclear reactions between the target nuclei and the radiation and a lot of data are reported in several databases both for neutrons and light charged particles [21, 22].

Not all databases are equally complete in the coverage of the relevant nuclides and energies for a specific application: in some cases the existing experimental data may be too scarce. Then, even if the relevant nuclides are covered by the database, they only assess the inclusive one-body cross sections and do not provide any information about correlations among particles produced by the same nuclear reaction.

Moreover, the knowledge of the total nuclear cross-section (σ_{tot}) is important for protons or helium and oxygen beams as well, since they have an important impact in the sophisticated features of therapy planning. The σ_{tot} provides essential information about the decrease of the fluence of primary beams and the release of secondary particles in the patient body. The impinging ions can produce exited nuclei with might then decay via β^+ or β^- with additional emission of a γ [23].

Regarding the proton beams, it is necessary to have information on target fragmentation, because it can modify the RBE of protons. However it is not always taken in account, because it is studied only using thin targets, that allow to detect low energy fragments (as the target fragments are), but do not allow a great interaction rate [13].

One of the goals of the FOOT experiment is to measure accurately the nuclear fragmentation with large statistics. For this reason instead of using very thin targets, it uses the inverse kinematic approach (discussed in Chapter 2), that greatly reduces the need to perform separate experiments. In fact, for example, cross section data for the reaction ^{4}He+^{12}C, can be used to study the reaction ^{12}C+^{4}He, too. However, the projectile energies will be different in each case [19].

Moreover, the two different FOOT setups (as explained in subsection 2.2.2) detect both heavy and light fragments for different beams and targets, collecting data also for Helium and Oxygen beams and focusing on the measurement of the differential cross section in function of the fragment energy. In fact, the final goal is to build a model for the treating planning system and a differential cross section is extremely necessary for this purpose.

3.2.1 Proton beams

The four important nuclei in medical applications are ^{1}H, ^{12}C, ^{16}O and ^{40}Ca. They are used as targets in case of proton beams.

To obtain information about the proton interaction mechanism with nuclei of atoms, total cross section from proton-induced reactions is useful. Until now, several experimental and theoretical studies on proton total cross sections have been performed.

Fig.3.7 shows the experimental data and the simulation about proton cross sections (p+p interaction), as do Fig.3.8 and Fig.3.9 for the two reactions p+^{12}C and p+^{16}O respectively.

The experimental data, reported as black dots, are collected from database of different and previous experiments, while the lines represent the Monte Carlo distributions of the considered process. These distributions clearly show that the data are more copious at low energy (below 50 MeV), while around the proton-therapy energy (around 200 MeV) are quite poor, in particular for Oxygen targets. Regarding a 200 MeV proton beam, the measurements of total cross sections are about 25 mb for the p+p reaction, 230 mb for the p+^{12}C reaction and 350 mb for the p+^{16}O reaction.

The cross section measurements and simulations, reported above, are related to the total reaction cross section, i.e. the probability that a certain reaction occurs at a fixed beam energy.

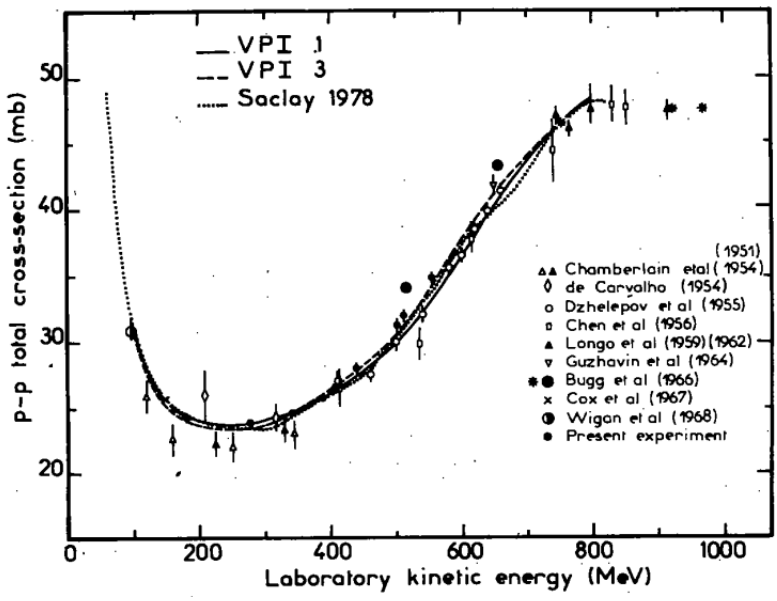

Figure 3.7: Total cross section of p+p reaction as function of the beam energy [24].

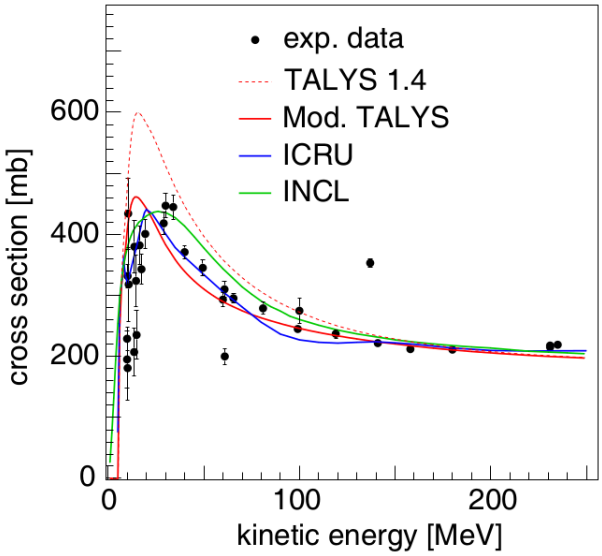

Figure 3.8: p+^{12}C cross section as function of the proton beam energy. Black dots are experimental data and colored curves are different MC simulation for comparisons [17].

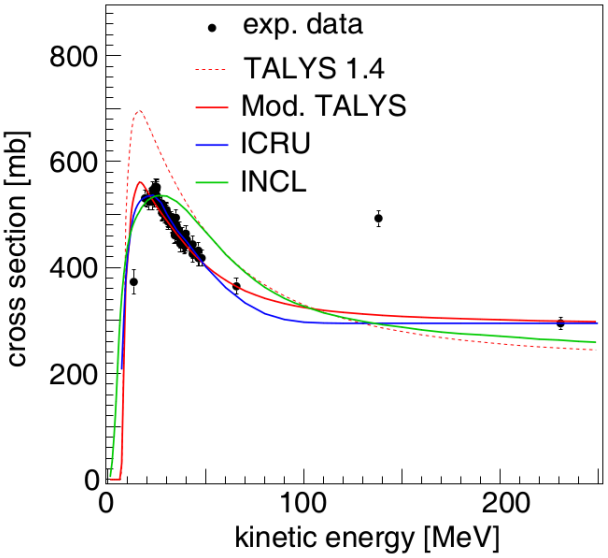

Figure 3.9: p+^{16}O cross section as function of the proton beam energy. Black dots are experimental data and colored curves are different MC simulation for comparisons [17].

For proton beams the angle-differential cross section (at different beam

energies and targets) has been measured as well, the experimental data are reported in Fig.3.10 as black dots, while the lines represent the Monte Carlo distributions of the considered process.

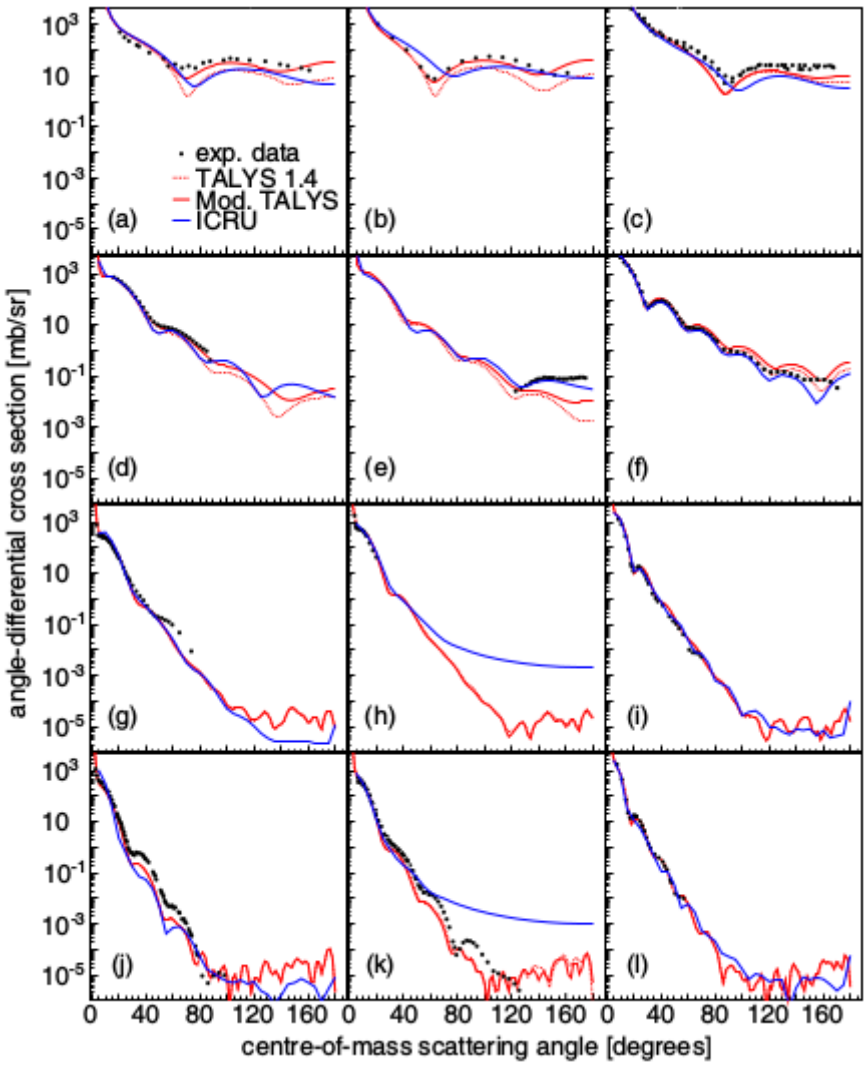

Figure 3.10: Angle-differential cross sections for proton beams at different energy and targets. The columns are referred to Carbon, Oxygen and Calcium respectively, while the rows are beams at different energies: 10 MeV (a,b,c), 50 MeV (d,e), 45 MeV (f), 140 MeV (h), 150 MeV (g,i), 200 MeV (k,l) and 249 MeV (j). The black dots are the experimental data while the distributions are different Monte Carlo simulation for comparisons.

What is missing in these data is the discrimination between different fragments, which is important in hadrontherapy to estimate biological damages and RBE variation after the Bragg peak.

In Tab.3.1 (reported at the end of this section) are summarized the previous data for proton-nucleus reactions, whereas there is not fragmentation for the p+p reaction. Moreover, the fragments studied as function of the beam energy are reported as well. The associated distributions, only for the p+^{12}C reaction, are shown in Fig.3.11 for lighter fragments and in Fig.3.12 for the heavier ones, compared with different Monte Carlo simulations.

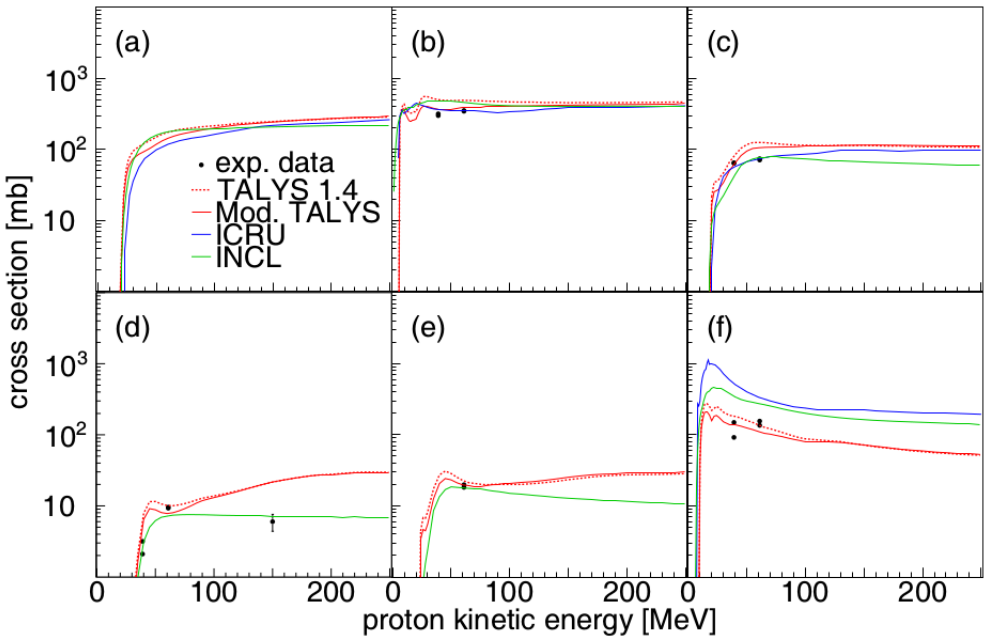

Figure 3.11: p+^{12}C cross section as function of the proton beam energy for the different fragments: neutrons (a), protons (b), deuterons (c), tritons (d), ^{3}He (e) and ^{4}He (f). The black dots are the experimental data while the distributions are different Monte Carlo simulation for comparisons.

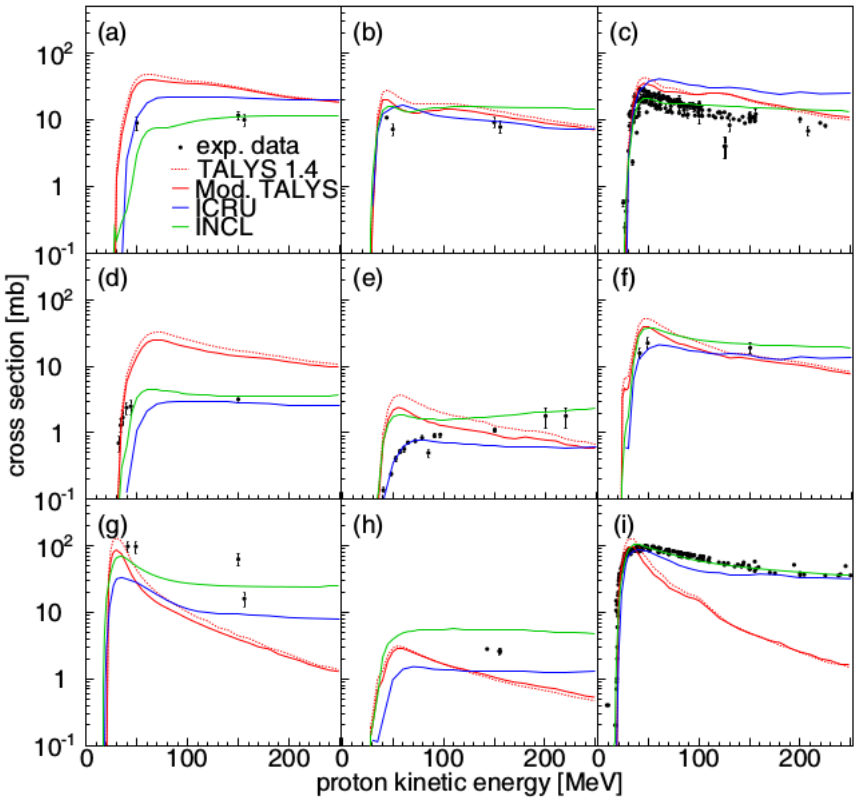

Figure 3.12: p+^{12}C cross section as function of the proton beam energy for the different fragments: ^{6}Li (a), ^{7}Li (b), ^{7}Be (c), ^{9}Be (d), ^{10}Be (e), ^{10}B (f), ^{11}B (g), ^{10}C (h), ^{11}C (i). The black dots are the experimental data while the distributions are different Monte Carlo simulation for comparisons.

First of all, the collected data are not enough for each fragment and so the experimental panorama is not complete for what concern the fragment discrimination. Therefore, a further step is required and it is one of the FOOT goals: it consists of discriminating the outgoing fragment not only as function of angle or beam energy, but especially with respect to the fragment itself and its energy (or momentum). The reason is that the depth-dose deposition in the human body depends on the fragment energy and its charge.

PROTON BEAMS			
Energy (MeV/n)	**Angle (degrees)**	**Target material**	**Detected fragments**
10 50 150 249	0-160 0-90 0-80 0-100	^{12}C	p, n, d, t, ^{3,4}He, ^{6,7}Li, ^{7,9,10}Be, ^{10,11}B, ^{10,11}C
10 50 140 200	0-160 120-160 0-30 0-130	^{16}O	p, n, d, t, ^{3,4}He, ^{6,7}Li, ^{7,9,10}Be, ^{10,11}B, ^{10,11,14}C, ^{13}N, ^{15}O
10 45 150 200	0-160 0-160 0-90 0-60	^{40}Ca	p, n, d, t, ^{3,4}He, ^{28}Si, ^{32}S, ^{36}Cl, ^{36,37,38}Ar, ^{38,39}K, ^{39}Ca

Table 3.1: Angle-differential cross section data for proton beams on different targets. Beam energies, emission angles and detected fragments are reported for each case.

3.2.2 Carbon ion beams

For the promising features already described at the beginning of this paragraph, the Carbon ions RBE has to be replaced by the one associated with the arising mixed radiation field (because the RBE depends on the LET, which is different for each isotope, as defined in Chapter 1). Moreover, the incident ions lose their energy passing through the patient body (up to 70% of energy for 400 MeV/u ^{12}C in water [25]) so that the inelastic nuclear reactions may occur at energies much lower than the incident ones.

Therefore, all these effects arising from the carbon fragmentation have to be considered and correctly evaluated when planning a tumor treatment [26].

The Carbon ion beams data at the hadrontherapy energies are several in literature, here a brief summary is reported (with a review in Tab.3.2 at the end of this section). At INFN-LNS facility in Catania, Italy, differential cross section data (shown in Fig.3.13) have been collected for a Carbon beam energy of 62 MeV/n and 80 MeV/n at different angles on ^{12}C-target [27], on ^{197}Au [28] and on a PMMA[1] target [29]. These energy are both too low to study fragmentation in case of hadrontherapy energies.

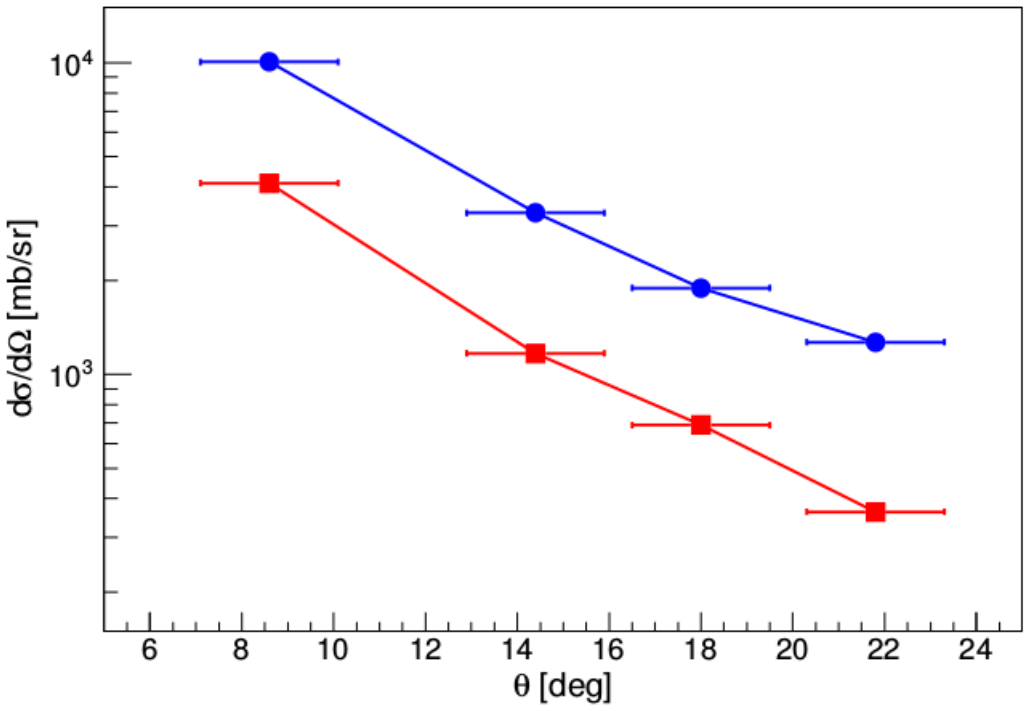

Figure 3.13: Angular differential cross sections for the ^{4}He production in the ^{12}C+^{12}C (red dots) and ^{12}C+^{197}Au (blue dots) reactions [28].

[1]Poly-Methyl-Methacrylate ($C_5H_8O_2$).

The most complete data collection have been made at GANIL, Grand Accélérateur National d'Ions Lourds (with SPIRAL2 experiment started in 2011), and at GSI thanks to the FIRST (Fragmentation of Ions Relevant for Space and Therapy) experiment. The fragment discrimination as a function of the scattering angle ($d\sigma/d\Omega$) were well measured both in SPIRAL2 and FIRST experiment.

SPIRAL2 took measurements to obtain the double differential fragmentation cross sections for 95 MeV/n Carbon ion beam on different thin targets at angles from 4 to 43^o [14].

The measurements were made for twenty different angles and five different targets leading to the double differential fragmentation cross sections of ^{12}C on hydrogen, carbon, oxygen, aluminum and titanium in fragmented particles, ranging from protons to carbon ion isotopes. These observations indicate that most of the emitted particles result from the projectile fragmentation during nuclear reactions. Moreover, the method used to combine the cross sections of composite targets to extract an elemental target (CH_2 and C to extract H) has been validated.

In order to complete these data, a new data collection has been performed on September 2013 to measure the fragmentation cross section at zero degree [25]. The angular distributions for the carbon target at GANIL (^{12}C+^{12}C reaction, with a beam energy of 95 MeV/n) are shown in Fig.3.14: one plot per Z is drawn, on which the different detected isotopes and their sum, including a measurement at zero degree angle value, are superimposed.

Whereas, the FIRST experiment has been designed for the measurement of ion fragmentation cross sections at different angles and energies (between 100 and 1000 MeV/nucleon).

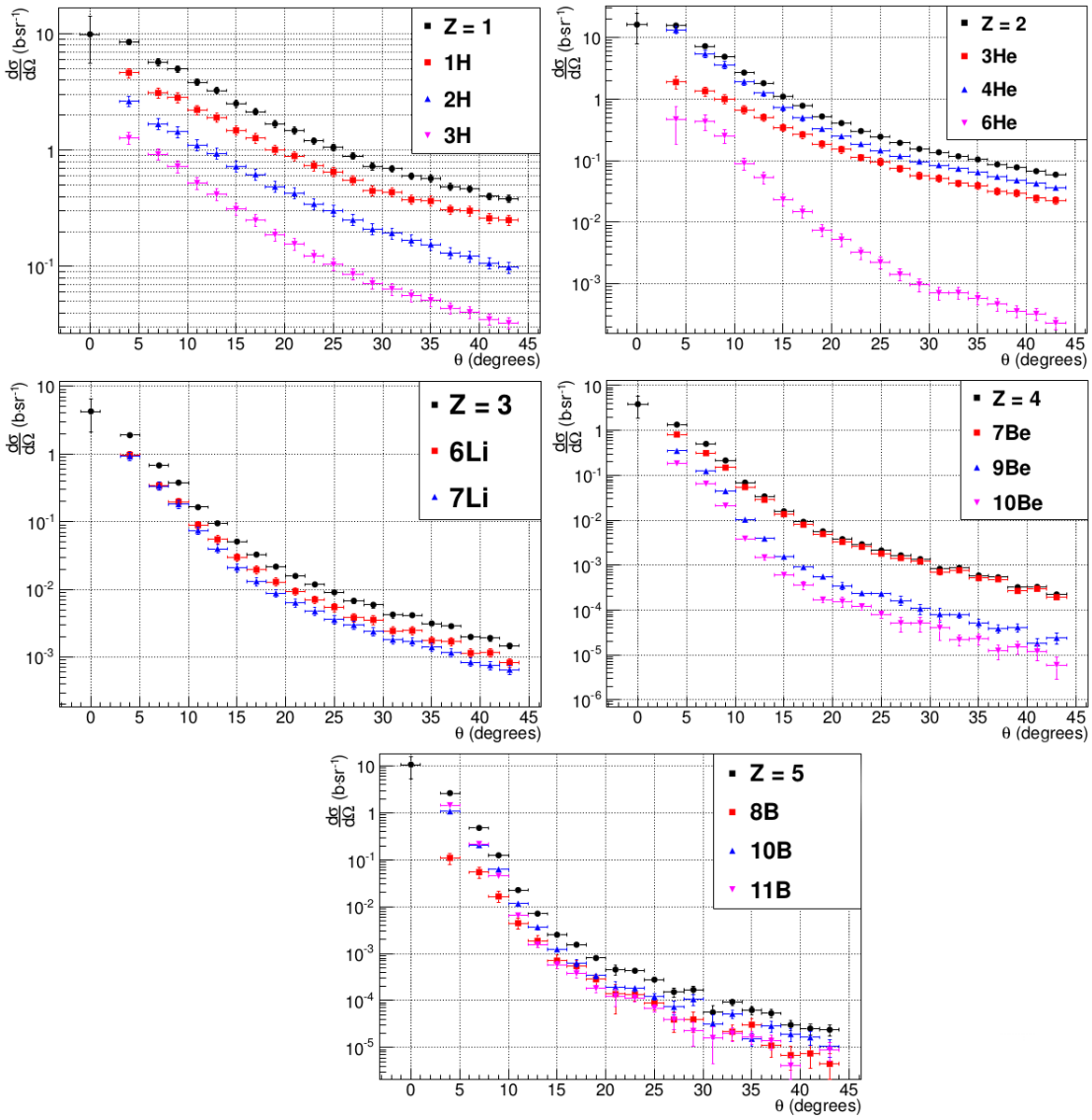

Figure 3.14: Angle-differential cross section for fragments resulting from the fragmentation on carbon target. Each graph represents the distribution per Z value.

The start of the scientific program of the FIRST experiment was on summer 2011 and the focus was on the measurement of 400 MeV/n ^{12}C beam fragmentation on thin (8 mm) graphite target [30].

The experimental setup was optimized to study two distinct angular regions: the small angle region, where fragments are produced with a polar angle θ with respect to the impinging beam direction smaller than 6^o [31] and a large angle region with $6 < \theta < 40$ degree. Regarding the bigger angles, data have been obtained by exposing two ECC (Emulsion Cloud Chamber, defined in paragraph 2.3.2) detectors to the beam, in order to collect fragments with a continuous angular distribution in the range 47^o-81^o with respect to the beam axis [20]. The measured differential cross sections, as a function of θ are shown in Fig.3.15: it can be noticed that while most of the fragments are emitted forward, a not negligible fraction of the light $Z = 1$, 2 fragments are produced with larger angles distribution.

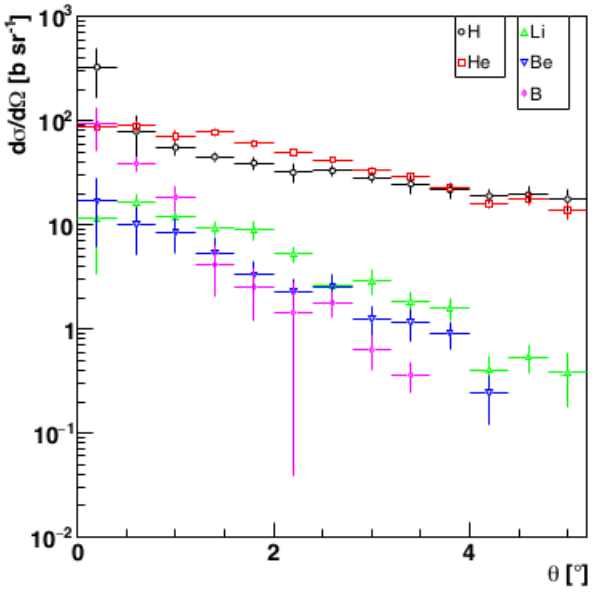

Figure 3.15: Fragmentation cross sections as a function of the fragment angle with respect to the beam axis, for H, He, Li, Be and B, measured by the FIRST experiment for the Carbon on graphite reaction. Light fragments are produces mostly at large angle distribution [32].

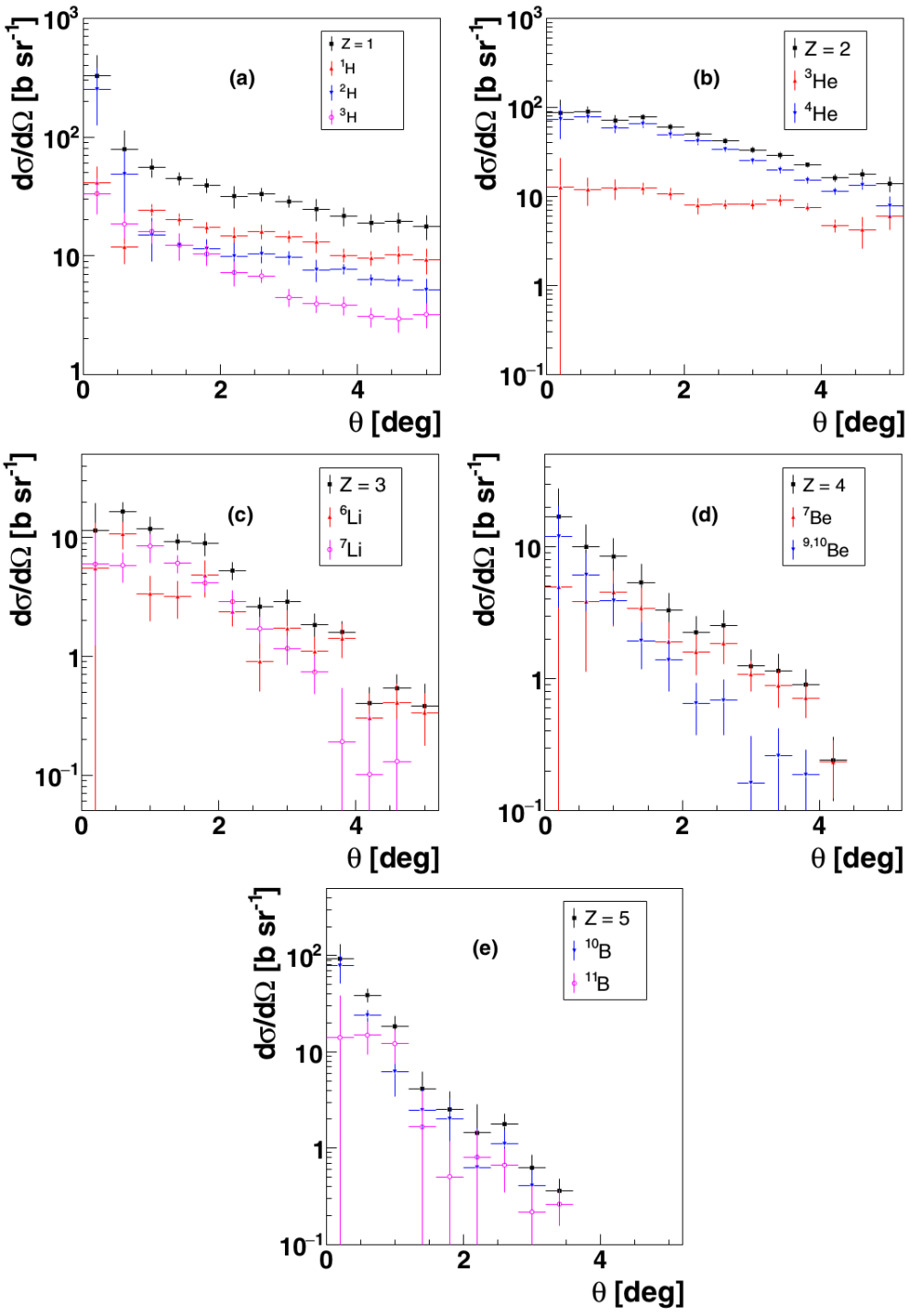

Figure 3.16: Angle-differential cross section for fragments resulting from the ^{12}C+^{197}Au reaction, where each plot represents the distribution per Z value.

Using the ECC technique, at the HIMAC facility in Chiba, Japan, a chamber made of Lexan[2] plates alternated with nuclear emulsion films was exposed to a Carbon ion beam. Lexan plates acted as passive material simulating human body tissues while nuclear emulsion films were used as both tracking devices with micrometric accuracy and ionization detectors. Such a detector allowed the detection of Carbon interactions produced along their path, the identification of the fragments produced and the measurement of their scattering angle. The results have been measured for the total and partial charge-changing cross-sections for $\Delta Z = 1, 2, 3, 4$. The corresponding cross-sections are [33]:

$$\sigma(\Delta Z = 1) = (2510 \pm 140_{stat} \pm 250_{sys})\,\text{mbarn};$$

$$\sigma(\Delta Z = 2) = (1170 \pm 90_{stat} \pm 120_{sys})\,\text{mbarn};$$

$$\sigma(\Delta Z = 3) = (1460 \pm 105_{stat} \pm 150_{sys})\,\text{mbarn};$$

$$\sigma(\Delta Z = 4) = (7510 \pm 240_{stat} \pm 750_{sys})\,\text{mbarn}.$$

Regarding the survival probability of the Carbon nuclei along the Chamber until the Bragg peak was found to be about 30%, i.e. only this percentage of Carbon ions arrives at the end of their range, while the complementary fraction interacts before.

The whole scenario of data collected by different experiments is shown in Tab. 3.2, using different targets and beams (described above), ordered by energy, from the lowest to the highest. It is easy to notice that the entire energy range for hadrontherapy is not covered (50-400 MeV/n for carbon ions), therefore a larger number of measurement is needed. It is important to point out that, as for proton beams, the fragment energy is not measured, moreover only the projectile fragmentation is considered. As discussed in the

[2]Lexan is a plastic material which belongs to the polycarbonates group.

previous chapter, the FOOT experiment is going to make measurements in inverse kinematic for considering and evaluating the target fragmentation as well.

^{12}C BEAMS			
Energy (MeV/n)	**Target material**	**Angles (degree)**	**Detected fragments**
62	^{12}C	2.2, 7.6, 14.4, 18	^{4}He, ^{6,7}Li, ^{7,9}Be, ^{10,11}B
		11.4, 14.4, 17.2, 19.4	p, d, t
	^{12}C, ^{197}Au	8.6	^{6,7}Li, ^{7,9}Be
		8.6, 14.4, 18, 21.8	^{4}He
80	PMMA	90	protons
95	H, C, O	$0 < \theta < 43$	^{1,2,3}H, ^{3,4,6}He
			^{6,7}Li, ^{7,9,10}Be, ^{8}B
			^{10,11}B, ^{10,11,12}C
	H, C	0	^{4}He, ^{6,7}Li, ^{7}Be
220	PMMA	60, 90	p, d, t
400	^{12}C	$\theta < 5$	H, He, Li, Be, B
	ECC	$47 < \theta < 81$	^{12}C
		$0 < \theta < 57$	$\Delta Z = 1, 2, 3, 4$

Table 3.2: Collected data about ^{12}C beams ordered by energy, for each energy are reported the target material, the angles at which the measurement was made and the fragments studied with the detection.

Chapter 4

The Acquisition System

The FOOT detector (described in Chapter 2) will be equipped with a Data Acquisition System (DAQ) designed to acquire the largest sample size of data with high accuracy in a controlled and online-monitored environment.

4.1 The DAQ Components

The FOOT experiment goals (as described in Chapter 2) are to measure the fragmentation of the projectile and the target for energies and materials useful in hadrontherapy. The collected data are needed to better plan the Treatment Planning System (TPS). To detect these fragments, the FOOT experiment need to provide the measurement of the following quantities:

- the momentum p of the outgoing fragments, with a resolution $\frac{\sigma(p)}{p} > 5\%$;
- the time of flight (TOF) of the fragments with a resolution of the order of 100 ps;
- the kinetic energy E_k of the fragments with a resolution $\frac{\sigma(E_k)}{E_k} \sim 2\%$;
- the stopping power ($\mathrm{d}E/\mathrm{d}x$) with a minimal resolution of the 2%.

The acceptance of the detector is limited to solid angles up to 10^o from the beam direction. This is enough to measure most of the heavy fragments produced on target. In the first region of the detector, the beam impinge on a plastic scintillator due to provide the trigger for the experiment and to measure the start for the TOF, thanks to four fast photomultipliers (PMTs), then it will pass through a drift chamber to track the direction and to monitor possible unwanted beam interactions in the scintillators. After these two detectors the beam will impinge on the target (the detector setup is in detail described in Chapter 2).

The beam and the fragments, produced in the target, will go through the Vertex Tracker (made up of pixel sensors of the MIMOSA28/Ultimate type and described in subsection 2.3.1) which can detect the position of each fragment.

After the Vertex Tracker, the particles pass through a magnetic region (0.8 T) spaced out with two Silicon pixel detectors. This tracking system needs to calculate the momentum p of the particles, knowing the relation $p = rqB$ (r is the curvature radius of the particle trajectory, q the particle charge and B the magnetic field). The fragments travel for about one meter in the air before impinging on a plastic scintillator, which measures the stopping power and provides the stop of the TOF. At last, there will be an inorganic scintillator (BGO, bismuth germanate) to measure the kinetic energy of the fragments.

The data have to be collected by a DAQ system, which need to have the following characteristics:

- the acquisition frequency must depend on the beam characteristic and the slowest detector rate. It is important not to have data or events overlapping;

- the acquisition system must work in different laboratories and conditions, therefore it is necessary to be easily configurable;
- the monitoring of the DAQ system must be possible during the acquisition (online), as well as the acquired data and information from each sub-detector.

For these reasons, the best estimated rate for the trigger is 1 kHz, because it depends on the slowest detector, that is the MIMOSA28 chips in the pixel tracker. Infact, it has a frame readout time of 180 μs, needed to readout about 10^6 pixels per chip. This detector fixes the overall maximum DAQ rate at about 5 kHz, but in order to reduce the effects of pile-up (the overlap of two different events), in the MIMOSA chips, the actual trigger rate will be of the order of 1 kHz.

In general, all the DAQ components need to be monitored during the acquisition. This control system will be hosted on a PC (Head PC) used to start/stop a single run, to check and to configure the acquisition system. While, another PC (Storage PC) will be used to collect the information coming from the different detectors and to store on disk the acquired data.

In Tab.4.1 the detectors that will be used in the experiment with the associated acquisition boards are reported. The readout systems are consists of standard VME boards placed in VME crates, so a Single Board Computer (SBC) is needed in each crate to dispatch DAQ commands on the different boards in the crate. As reported in Tab.4.1, the estimated event data size is of the order of 22 kB to be acquired at an average rate of 1 kHz (as explained above). This fixes the capability of the system at the Storage PC to be of the order 22 MB/s on average.

Detector	Board Type	Max Event Rate	Event size
Trigger	V2495	10 kHz	40 B
Start Counter	DreamWave	1 kHz	8.2 kB
Beam Monitor	TDC	5 kHz	0.1 kB
Vertex Detector	SoC on DEx	2 kHz	0.9 kB
Inner Tracker	SoC on DEx	2 kHz	2.1 kB
Outer Tracker	Custom	2 kHz	0.5 kB
ΔE/Δx	DreamWave	1 kHz	8.4 kB
Calorimeter	QDC	2 kHz	1.7 kB
Total DAQ	Storage PC	1 kHz	$\sim$22 kB

Table 4.1: List of the detectors with the associated DAQ boards, the maximum event rate and the event size. CAEN V2495 is the trigger board, SoC stands for System-On-Chips, TDC is a Time to Digital Converter and QDC, Charge to Digital Converter [12].

At the moment, the preliminary tests are made on a first simple setup that contains only the trigger, a flash ADC[1] (connected to two PMTs, which read two scintillators) and the Vertex detector. In particular, the scintillators collect data (for now by cosmic rays) and the PMTs produce a voltage signal which is sent to the trigger board and to the flash ADC, which converts the signal from the event in a digital signal, easy to be stored and read by the acquisition software. The trigger is also connected to the Vertex board (see the subsection 4.1.3) that, for now, produce the same kind of data as the vertex detector.

[1] Analog to Digital Converter

4.1.1 The trigger

The trigger system task is to send a signal to the DAQ components, each time a particle passes through the Start Counter (SC). This sets the start of an event and, by consequence, of the system.

The trigger board (CAEN V2495, shown in Fig.4.1) will receive four logic signals from the four PMTs of the detector and one signal from each detector with its DAQ status: IDLE, ready to acquire, or BUSY, still reading the previous event. A schematic view of the trigger input and output signals is shown in Fig.4.2.

In particular, the trigger signal will be obtained asking for at least a time coincidence between two PMT signals within a gate of 20 ns. Then, the trigger signal will be broadcasted to all detectors only if all the detectors will be at the IDLE status [12].

It is also extremely important to collect information from DAQ system itself: its time (in clock ticks) and live time since the previous trigger, PMT signal counters and information on the BUSY status of the sub-detectors. All these information are very useful in the DAQ monitoring system for checking the synchronization and the consistency of the data acquired.

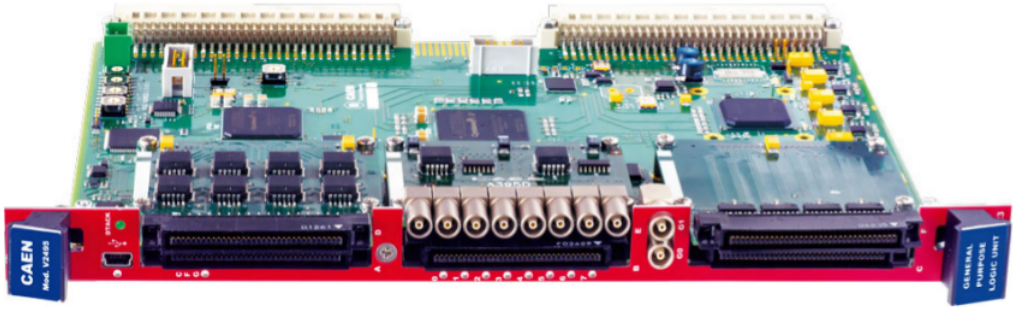

Figure 4.1: The trigger board CAEN V2495.

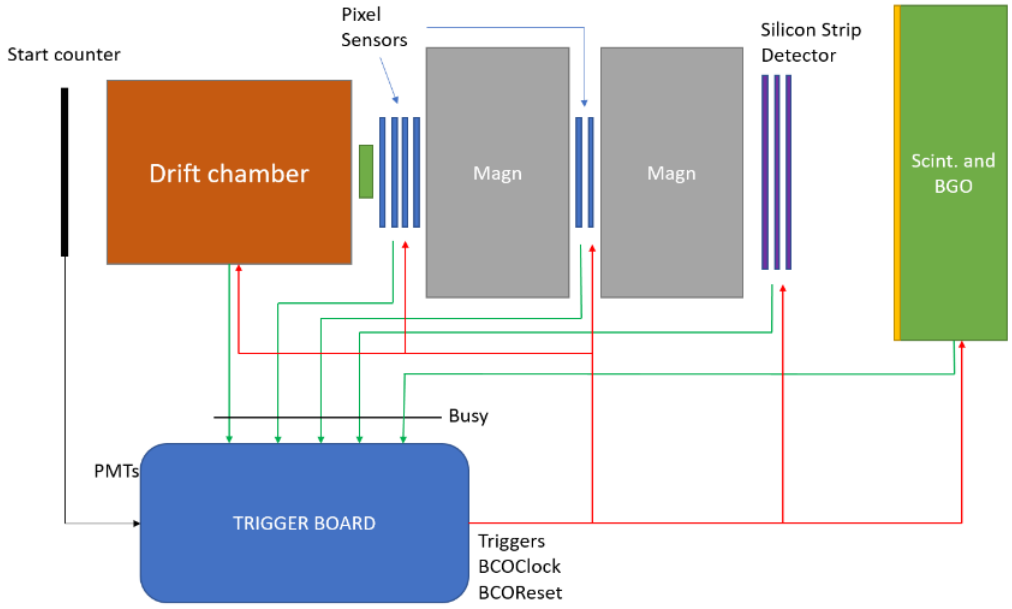

Figure 4.2: Schematic view of the DAQ components and the connection between them and the trigger.

4.1.2 The flash ADC

The flash ADC board is a CAEN V1720 board (Fig.4.3), which is used to store the acquired events.

When the acquisition is running, a trigger signal allows to increment the Event Counter and to fill the active buffer with the data. An event is therefore composed by the data and the event counter. A trigger signal can be refused if the memory is full and therefore there are no available buffers or if the trigger overlaps the previous one and the board is not enabled for accepting overlapped triggers [34].

The registered event has a standard structure: the header of the event contains the information about the number of channels that have been used (for a maximum of 8), the number of words for each channel and the event

number. The header is followed by the acquired data itself (like the voltage values from the PMTs connected to the two scintillators).

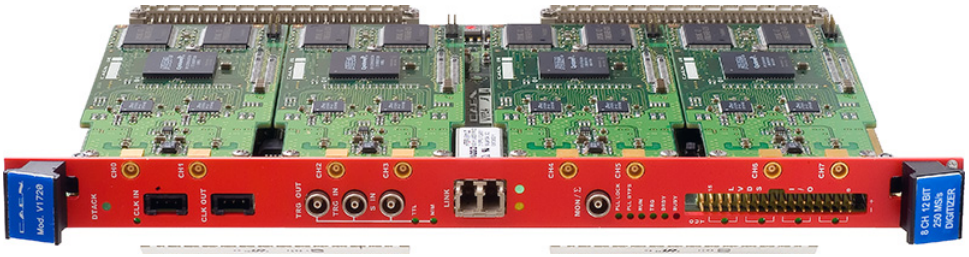

Figure 4.3: The flash ADC board CAEN V1720.

4.1.3 The vertex detector

The Vertex Tracker may contain up to four different Silicon pixel layers, which allow to detect particles with an emission angle in the range of $\pm 40^o$ with an efficiency higher than 95%. Measuring the particle position in four different points, it is possible to determine the trajectory of the particle. The MIMOSA28 (a picture of the M28/Ultimate chip is shown in Fig.4.4) is formed by a 928x960 pixels matrix and it belongs to the MAPS-CMOS type (Monolithic Active Pixel Sensors – Complementary Metal-Oxide Semiconductor).

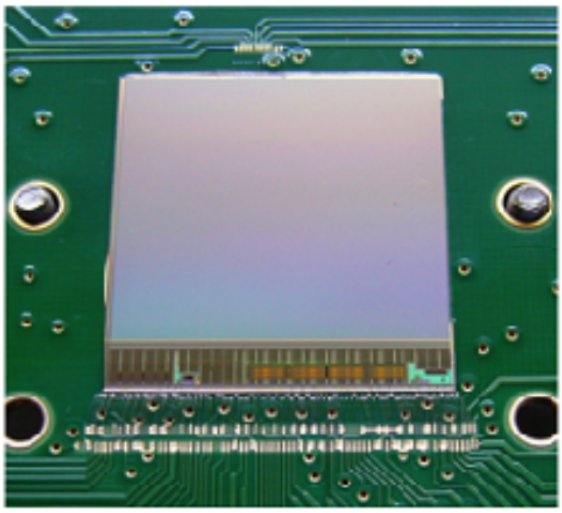

Figure 4.4: MIMOSA28/Ultimate chip used in the Vertex DAQ board.

4.2 The DAQ Interface

The DAQ system contains different elements for the whole data acquisition; in Fig.4.5 the logical structure of the DAQ system with the control PC on top and all the distributed DAQ elements and devices is shown. The detector elements are directly connected with electronic boards residing on custom or VME crates or on PCs, which are handled by software modules called generically "Readout Modules". These software elements are responsible for configuration of the detectors and of the electronics and of the data read-out. All the collected data are saved in the PC Storage that receives data via different methods, depending on the sub-detectors (fiber or ethernet connection). Stored data will be sent to different PCs in order to constantly monitor the sub-detectors and to a PC needed for the general monitoring of the whole systems [35].

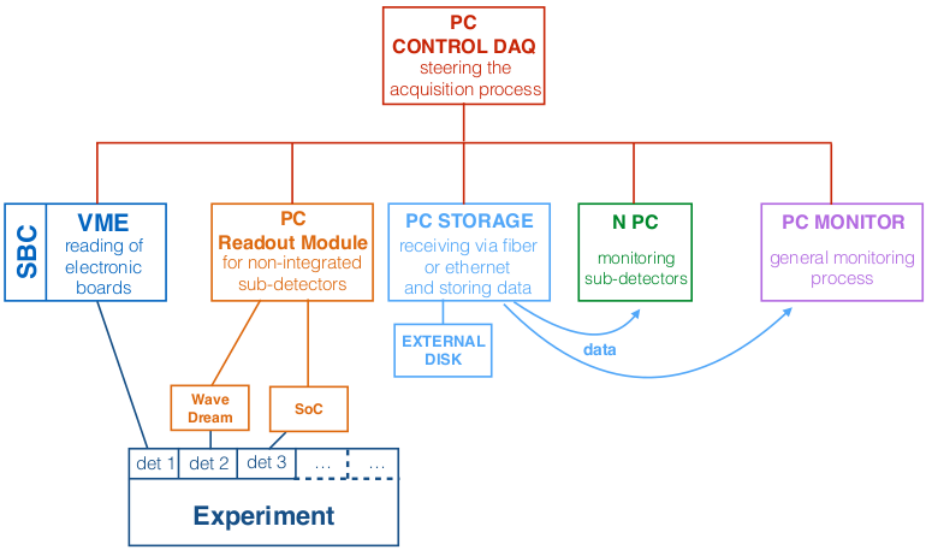

Figure 4.5: DAQ interface and system scheme.

In a DAQ system, a set of data sources can be combined between them to build events from different sub-detectors or parts of them. All streams of data need to be handle by a software, which also shows online information about the run for monitoring its acquisition. The DAQ system will provide several sets of online monitoring information. Simple information pieces on the DAQ running can be collected from each VME board or device at a monitoring rate (each 10 s [12]) and provided to the network of PCs connected to the experiment.

The FOOT TDAQ Software runs on the PC Control DAQ, which talks to the other devices through the software itself using a finite-state machine (FSM) to describe the current status of the DAQ. It is a logical machine that can change from one state to another in response to some external inputs; the change from one state to another is called a transition. The state transition of a FSM corresponds to some methods, called in all the Readout Modules present in the DAQ system, which determine the state itself. The

FOOT DAQ Software interface is shown in Fig.4.6: the various transitions are on the left side with the current DAQ state (in this case RUNNING), while on the right there are the logical view of the system. In the lower part of the interface the Error Reporting System (ERS) shows the information on warnings or errors during the transitions or the running state. During the run time the Readout System (ROS) delivers fragments data (or releases fragments) only when triggered by an external demand.

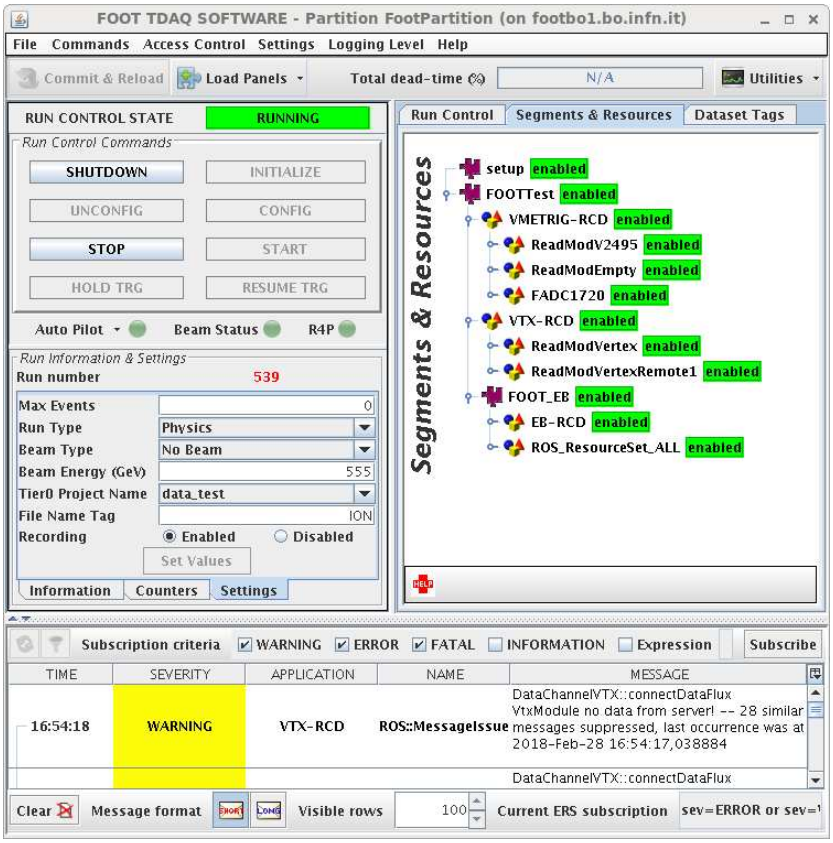

Figure 4.6: FOOT DAQ Software interface: in this case the DAQ state is RUNNING. In the lieft side of the interface the possible transitions are listed: in black the possible ones and in light gray the forbidden transitions from the present status. On the right side, system segments are shown with their own status.

First of all, a configuration for the system has to be decided, then the machine status can be lead to the running state . In detail, the possible transitions are [36, 37]:

- INITIALIZE: initializes any software packages required for operating, starts online system infrastructure and all supervised processes;
- CONFIG: prepares for the running state, i.e. reads required parameters, starts any required processes and configures every device;
- START: brings the state to running;
- STOP: exits from the state of running;
- UNCONFIG: deletes the previous configuration for preparing the system for a new one;
- SHUTDOWN: stops all the supervised processes.

Moreover, in Fig.4.6 it is possible to read the logical view of the system (on the right), where the different data and information sources are listed: the two ROD Crate DAQ, VMETRIG-RCD and VTX-RCD, corresponds to two different CPUs collecting data from two sets of electronic boards. A third element in the system, FOOT_EB, the FOOT Event Builder, corresponds to a third PC where event fragments coming from the previous CPUs are collected and used to build the final event, which is then stored locally.

4.3 Event Building and Storage

In the distributed environment where the DAQ operates, each detector provides information at each issued trigger and the data from all detectors

are collected in the storage PC. A critical point of the whole data taking is the synchronization of all detectors and the build-up of the events, putting together fragments related to the same trigger.

The events collected are stored in files, tagged by their run numbers. To maximize the DAQ rate, the events are first stored on a Solid State Drive (SSD), which has a maximal bandwidth of 400 MB/s and are later transferred to a local raid 5 system, taking advantage of any stop or dead time of the DAQ.

4.3.1 The raw data files and event format

This paragraph describes the raw event format, based on ATLAS Trigger and DAQ document [38].

The basic unit of the raw data file is a *fragment* and each fragment has a header, a sample of data and a tail. The header marks the fragment type, the data are the information included in the fragment (as the event size, the acquisition time or the collected data themselves, etc.) and the tail marks the end of that fragment.

The raw data file starts with a first fragment called **Header**, where the general information, like the file name or the file size, are included. Then, there is one fragment for each **Full Event**, i.e. an aggregation of ROB[2] fragments, each of which contains ROD[3] fragments [39]. At last, there is the **tail** of the file, which indicates that the end of file is reached.

The Start of Header Markers allows the identification of the fragment (header markers of fragment type cited above are reported in Tab.4.2). The same happens in the ROD fragment, which is formed by the event fragments

[2]Readout Buffer

[3]Readout Drivers

(each for every acquisition board connecting at the same ROB).

Fragment Type	Header Marker
Full Event	0xaa1234aa
ROB	0xdd1234dd
ROD	0xee1234ee

Table 4.2: Start of header markers to identify the start of every new event with its inner partition [38].

At the moment, the raw data file contains only information from the trigger board, two empty channels (needed to simulate different devices that are going to be add later on in the acquisition system), the Flash ADC and the Vertex detector data. In particular first ROB includes the Trigger, the Empty and the Flash ADC fragments, while in a second one there are another Empty fragment and the Vertex Tracker fragment.

Each of these file fragments starts with the **Source identifier**, which consists of a 32 bits word coded in this way:

- bits 31-24 are optional and often set to zero;

- bits 23-16 contains the so called "Sub Detector ID" which is a tag of a part of a general apparatus;

- bits 0-15 contains the unique identification of the specific electronic board that gave origin to the data that will follow.

In FOOT, all electronic boards are associated to the same Sub Detector ID, which is fixed to the hexadecimal number 82 and boards of the same type will have the same bits 8-15. Bits 0-7 are used to identify each board individually, see for example Tab.4.3.

Devices	Board Name	Channel ID
Trigger	V2495	0x00828044
Empty 1	-	0x00828701
Flash ADC	V1720	0x00828901
Empty 2	-	0x00828703
Vertex Detector	MIMOSA28/Ultimate	0x00828706

Table 4.3: Source identifiers for each DAQ device, useful for their identification during the file reading for the acquisition online monitoring functions.

4.4 The Event Reading Code

The goal of this thesis work is to provide a `C++` code able to read and decode the raw data file. This code is an important connection between the DAQ system and the tracks reconstruction algorithm, which is currently working with Monte Carlo simulated data. Infact, thanks to the decoded raw data file, the reconstruction algorithm will read the real acquired events and will use them for extracting physics information about the produced nuclei during the projectile-target interaction.

The algorithm decodes the raw data file looking for the Header Markers of the full event, the ROB and the ROD (reported in Tab.4.2) and the Source identifier (Tab.4.3) for distinguishing the different fragments from the different DAQ boards. Each of these fragments, from a different device, is linked to a `struct`[4] in the code. Each `struct` contains the needed variables for reading a fragment, in such a way that each variable is associated to one information written in the raw data file by the respective board.

These structures are fundamental for the off-line events and tracks recon-

[4]In `C++` a structure (struct) is a group of variables, even of different type, put together in the same family with the same name.

struction, because they will be implemented into the reconstruction FOOT software (SHOE). For these reasons, the code, developed in this thesis, has two contemporary important applications: reading and decoding the raw data file to prepare the data for the analysis and to monitor the acquisition itself.

At the moment, the code contains six structures (`struct`), one for each type of fragment: the header (repeated once in the file beginning) and the various fragments of the full event (repeated until the end of the file, i.e. for the all acquired full events in that run). In Tab.4.4 are reported the `struct` names associated to the board fragments and the saved information for the monitoring. The event data from the flash ADC and the Vertex Tracker are also read by the code, but not printed, even though the structures are able to read and save these data for the following analysis and reconstruction.

The variables contained in these structures are used in different functions in the code (one function for each struct). A function reads its corresponding fragment and associates the right word to the right variable, which is printed in the output.

The whole assemble of functions and structures is included in a `class`, named `EventReader`, which is partially shown in Fig.4.7. The aim is to show the basic function of the code, which are those for opening (`OpenFile`) and closing (`CloseFile`) the encoded file, i.e. mandatory function for reading the file; the `getNextEvent` is the cycling function for reading each single event until the file ends (`EndOfFileReached`). Moreover, in Fig.4.7 also the pointers for each structure are reported.

Two printed output examples are reported as well: in Fig.4.8 the header information are shown and in Fig.4.9 the full event ones (the same screen is reported for two event data, for the event zero and the event five, to give an

example).

```
class EventReader {

public:

  EventReader();
  ~EventReader();

  bool OpenFile( std::string filename );

  void CloseFile();

  void getNextEvent();

  bool EndOfFileReached();

private:

  InfoHeader* head;
  InfoEvent* info;
  TrgEvent* trg;
  EmptyEvent* empty1;
  fADCEvent* fADC;
  EmptyEvent* empty2;
  VTXEvent* vtx;
};
```

Figure 4.7: A part of the header file, reduced at minimum, of the developed `class EventReader`, with its public function members and the private ones (pointers for each structure).

```
------------------HEADER OF FILE--------------------
Info Header one, WRITER=: EB-RCD
Info Header two, FILENAME=: data_test.00000460.physics_foot.daq.RAW._lb0000._EB-RCD
Info Header three: GUID=1E3AF79F-250B-E811-8C5C-38D54715E46E
Info Header four: Stream=physics_foot
Info Header five: Project=data_test
Info Header six: LumiBlock=0
------------------END OF HEADER FILE----------------
```

Figure 4.8: The printed output of the header information in the raw data file.

```
INFO and DATA about Event Number: 0
Buch Crossing Time in Seconds: 1517911687
Bunch Crossing Time in NanoSeconds: 88250000
Run Type (hex): f
Run Number: 460
Extended Level 1 ID: 1120

TRIGGER DATA:
Channel ID (hex): 828044
Time in Seconds: 1517907871
Time in MicroSeconds: 307024
Number of Event: 0
Live Time (clock periods): 39663916
Clock Counter: 39668913
Time since last Trigger: 39668911
Event Counter: 0
BCO of Trigger: 396680
Trigger Delay: 19
PMTs & Busy: 992

EMPTY DATA FIRST ROB:
Channel ID (hex): 828701
Time in Seconds: 1517907871
Time in MicroSeconds: 307477
LumiBlock Number: 762541165
Event Number: 0

FLASH ADC DATA:
Channel ID (hex): 828901
Number of Event_: 0
Number of channels: 2

EMPTY DATA SECOND ROB:
Channel ID (hex): 828703
Time in Seconds: 1517907953
Time in MicroSeconds: 179101
LumiBlock Number: 214032
Event Number: 0

VERTEX DATA:
Channel ID (hex): 828706
Time in seconds: 1517907953
Time in microseconds: 179142
Lumi Block: 265184
Number of Event: 0
EVENT COUNTER: 0
```

```
INFO and DATA about Event Number: 5
Buch Crossing Time in Seconds: 1517911692
Bunch Crossing Time in NanoSeconds: 86344000
Run Type (hex): f
Run Number: 460
Extended Level 1 ID: 1126

TRIGGER DATA:
Channel ID (hex): 828044
Time in Seconds: 1517907873
Time in MicroSeconds: 259197
Number of Event: 5
Live Time (clock periods): 58883356
Clock Counter: 234906687
Time since last Trigger: 59158672
Event Counter: 5
BCO of Trigger: 2349057
Trigger Delay: 167
PMTs & Busy: 992

EMPTY DATA FIRST ROB:
Channel ID (hex): 828701
Time in Seconds: 1517907873
Time in MicroSeconds: 259326
LumiBlock Number: 762541165
Event Number: 5

FLASH ADC DATA:
Channel ID (hex): 828901
Number of Event_: 5
Number of channels: 2

EMPTY DATA SECOND ROB:
Channel ID (hex): 828703
Time in Seconds: 1517907958
Time in MicroSeconds: 180044
LumiBlock Number: 214032
Event Number: 5

VERTEX DATA:
Channel ID (hex): 828706
Time in seconds: 1517907958
Time in microseconds: 180049
Lumi Block: 265184
Number of Event: 5
EVENT COUNTER: 5
```

Figure 4.9: The printed output of the full event information, divided in each board data fragments. The examples for the event number zero and number five are reported.

Fragment	Struct Name	Acquired information
File Header	InfoHeader	Writer
		Filename
		Project
Full Event Header	InfoEvent	Bunch crossing time
		Run type
		Run number
Trigger data	TrgEvent	Channel ID
		Time in seconds and microseconds
		Event number
		Live time (in clock periods)
		Time since last trigger
		Event counter
Empty data	EmpyEvent	Channel ID
		Time in seconds and microseconds
		Event number
Flash ADC data	fADCEvent	Channel ID
		Event number
		Number of active channels
		Active channel sampled data
Vertex Tracker data	VTXEvent	Channel ID
		Time in seconds and microseconds
		Event number
		Event counter
		Detector hits

Table 4.4: `Struct` list from the acquisition control code: each fragment with its associated `struct` name and the important board information for the DAQ system check.

4.4.1 The acquisition control code

As described above, the C++ code developed in this thesis has the important function to monitor and debug the acquisition system. During this preliminary phase of DAQ development a check on each event is strictly necessary to be sure that the event is composed by consistent fragments of data (that means from the same trigger signal).

The whole acquisition system needs to be perfectly synchronized for allowing a free errors acquisition and data reading. It is important to distinguish the different events and to assign every fragment to the corresponding interaction event, that is the reason why the printed information (reported in Tab.4.4) are mostly times and numbers of event.

In particular, the first step of the test has been to compare the Event Number of each fragment for every event (on different raw data files) to verify the consistency. The Event Number information derives from the acquisition software, which connects with the device and write the received data. One of each data is instead the Event Counter, that is the number of the event measured by the board itself. The second step was to compare the Event Number with the Event Counter of the trigger and for the Event Number of the different devices.

In the case one of these relations (between the number of events) is not satisfied, the code will print in the output a *warning* message. This monitoring test has permitted to find and to fix some synchronization errors in the acquisition between the different devices and to optimize the system which is now more stable and robust.

Conclusions

The current thesis work has been performed within the FOOT collaboration, whose experiment aims at improving the knowledge of the nuclear phenomena that are relevant in the field of the hadrontherapy. This is an oncological cure, complementary to the standard ones (surgery, chemiotherapy or radiotherapy) which is particularly effective on specific cancer types (well localized) and is almost the unique non-invasive cure for particular cancer types (glaucoma or brain tumors).

One of the problems that has to be addressed with this technique is the accuracy of the Treatment Planning System (TPS) for which the dose deposition needs to be well known. At the present there are few data for the cross sections of fragments in the interested energy range.

In this work the current scientific panorama regarding the hadrontherapy energy beams and tissue targets is reported. It has been shown that to improve the TPS more data on the relevant cross sections at hadrontherapy energies are needed and the FOOT experiment will address this issue.

At the moment, the FOOT acquisition system is under development and preliminary tests are necessary for building a stable and reliable control system for monitoring the acquisition during the data collection, in particular the synchronization between the trigger and the other devices. Therefore, to address this point, a `C++` code has been built with a set of classes and struc-

tures able to read the raw data files that are written by the DAQ system.

This code will be extremely useful for the reconstruction software of the FOOT Experiment (SHOE): the plan is to integrate the functionalities developed in this thesis into the official framework to guarantee a consistent data reading and reconstruction software. In addiction, the code is the base of programs devoted to the checks of the integrity and consistency of the acquired data. They have already permitted the identification and the resolution of some synchronization errors during the acquisition.

The work presented in this thesis is, therefore, a mandatory requirement both for a better reconstruction of experimental data and for a stable and synchronized acquisition system.

Bibliography

[1] U. Amaldi: *"History of Hadrontherapy in the world and Italian developments"*, Rivista Medica, **72**, (7-22), 2008.

[2] R. Wilson: *"Radiological Use of Fast Protons"*, Radiology, **47**, (487-491), 1946.

[3] U. Amaldi: *"Particle Accelerators: from Big Bang Physics to Hadron Therapy"*, Geneve, Springer, 2015.

[4] W. R. Leo: *"Techniques for nuclear and particle physics experiments: A how-to approach"*, Berlin, Springer-Verlag, 1994.

[5] E. B. Podgorsak: *"Radiation in Physics for Medical Physicists"*, Montreal, Springer, 2016.

[6] R. Serber: *"Nuclear reactions at high energies"*, Physical Review, **72**, (1114–1115), 1947.

[7] J. D. Bowman, W. J. Swiatecki and C. F. Tsang: *"Abrasion and ablation of heavy ions"*, LBL Report No LBL-2908 University of California, (unpublished), 1973.

[8] D. Schardt et al.: *"Heavy-ion tumor therapy: physical and radiobiological benefits"*, Rev. Mod. Phys., **82**, (385-425), 2010.

[9] T. Terasawa et al.: *"Systematic review: Charged-particle radiation therapy for cancer"*, Annals of Internal Medicine, **151**, (556–565), 2009.

[10] M. Beyzadeoglu, G. Ozyigit and C. Ebruli: *"Basic Radiation Oncology"*, Berlin, Springer-Verlag, 2010.

[11] H. Tsujii et al.: *"Overview of Clinical Experiences on Carbon Ion Radiotherapy at NIRS"*, Radiotherapy and Oncology, **73**, (41-49), 2004.

[12] A. Alexandrov et al.: *"FOOT Conceptual Design Report"*, (1-94), 2017.

[13] F. Tommasino and M. Durante: *"Proton Radiobiology"*, Cancers, **7**, (353-381), 2015.

[14] J. Dudouet et al.: *"Double-differential fragmentation cross-section measurements of 95 MeV/nucleon ^{12}C beams on thin targets for hadron therapy"*, Physical Review C, **88**, 2013.

[15] G. De Lellis et al.: *"Emulsion Cloud Chamber technique to measure the fragmentation of high-energy carbon beam"*, Journal of Instrumentation, **2**, (1-6004), 2007.

[16] C. Agodi et al.: *"Heavy Ions Fragmentations Measurements at intermediate energies in hadrontherapy and spatial vehicles shielding "*, IEEE, **15**, (790-792), 2007.

[17] B. Braunn et al.: *"Assessment of nuclear-reaction codes for proton-induced reactions on light nuclei below 250 MeV"*, European Physical Journal-Plus, **130**, (1-18), 2015.

[18] M. Enferadi et al.: *"Nuclear reaction cross sections for proton therapy applications"*, J Radioanal Nucl Chem, **314**, (1207–1235), 2017.

[19] J. W. Norbury et al.: *"Review of Nuclear Physics Experiments for Space Radiation"*, NASA Technical Paper-217179, 2011.

[20] A. Aleksandro et al.: *"Measurement of large angle fragments induced by 400 MeV n^{-1} carbon ion beams"*, Measurement Science and Technology, **26**, (1-6), 2015.

[21] ICRU: *"Nuclear Data for Neutron and Proton Radiotherapy and for Radiation Protection"*, Report 63, 2000.

[22] A. Stankovskiy et al.: *"International Conference on Nuclear Data for Science and Technology 2007"*, EDP Sciences, **1**, (1387-1389), 2008.

[23] W. Ulmer et al.: *"A new calculation formula of nuclear cross-section of therapeutic protons"*, Journal of Proton Therapy, **1**, (1-11), 2015.

[24] P. Schwaller et al.: *"Proton total cross sections on ^{1}H, ^{2}H, ^{4}He, ^{9}Be, C and O in the energy range 180 to 560 MeV"*, Nuclear Physics, **A314**, (317-344), 1979.

[25] J. Dudouet et al.: *"Zero degree measurement of ^{12}C fragmentation at 95 MeV/A on thin targets"*, arXiv:1407.0223v1, 2014.

[26] S. Tropea et al.: *"Measurement of fragment production cross sections in the ^{12}C+^{12}C and ^{12}C+^{197}Au reactions at 62 A MeV*

for hadrontherapy and space radiation protection", Acta Physica Polonica B, **45**, (565-569), 2013.

[27] M. De Napoli et al.: *"Carbon fragmentation measurements and validation of the Geant4 nuclear reaction models for hadrontherapy"*, Physics in Medicine & Biology, **57**, (7651-7671), 2012.

[28] M. De Napoli et al.: *"Carbon Fragmentation Cross Sections for Hadrontherapy and Space Radiation Protection"*, Nuclear Data Sheets, **119**, (273-276), 2014.

[29] C. Agodi et al.: *"Charged particle's flux measurement from PMMA irradiated by 80 MeV/u carbon ion beam"*, Physics in Medicine & Biology, **57**, (5667–5678), 2012.

[30] R. Pleskac et al.: *"The FIRST experiment at GSI"*, Nuclear Instruments and Methods in Physics Research A, **678**, (130-138), 2012.

[31] M. Toppi et al.: *"Measurements of ^{12}C ion fragmentation on thin carbon target from the FIRST collaboration at GSI"*, Journal of Physics: Conference Series, **590**, (1-4), 2015.

[32] M. Toppi et al.: *"Measurements of ^{12}C ions fragmentation cross sections on a thin gold target with the FIRST apparatus"*, Proceedings of Science, **035**, (1-10), 2016.

[33] G. De Lellis et al.: *"Measurement of the fragmentation of Carbon nuclei used in hadrontherapy"*, Nuclear Physics A, **853**, (124–134), 2011.

[34] CAEN User Manual: *"V1720/VX1720 – 8 Channels 12bit 250 MS/s Digitizer"*, UM3051, 2017.

[35] Atlas: *"ATLAS TDAQ Readout, ROD Crate DAQ User's Guide"*, ATL-DQ-EN-0020, 2006.

[36] H. J. Burckhart, M. Caprini and R. Jones: *"Connection DCS ↔ DAQ in ATLAS"*, ATLAS Internal Working Note, 1999.

[37] Atlas: *"Large Scale Functionality and Performance Tests July 2005"*, ATL-D-TR-0003, 2005.

[38] C. Bee et al.: *"The raw event format in the ATLAS Trigger & DAQ"*, ATLAS Trigger & DAQ, ATL-D-ES-0019, 2011.

[39] Atlas: *"High-Level Trigger, Data Acquisition and Controls"*, Technical Design Report, ATLAS TDR-016, 2003.

Acknowledgements

First of all, I would like to express my gratitude to my surpervisor, Professor Mauro Villa, and to Silvia Biondi for their availability and their patience in giving me all the explanations and clarifications that I needed. I also thank Professor Roberto Spighi for all the advice and for leading me in this thesis work.

I thank my parents, Giuseppe and Daniela, for allowing me to enjoy my university years and for trusting me even though my life has always been full of 'I don't know's: starting from that question in kindergarten when I was asked who lived in a castle. As then, there are too many options in my mind and I can't pick one because I don't want to waste any chance. Don't worry, I will figure out my life sooner or later, but in the meantime there are going to be so much more 'I don't know's to fill the universe with, sorry!

Then, I really want to thank my aunt Silvia for teaching me to think outside the box, but most of all for teaching me the real meaning of 'living'. Thanks for always letting me talk and for listening to me about my doubts, thoughts and opinions, without ever judging me.

I have to express my heartfelt gratitude to all my physics collegemates of these 5 years and especially who also shared these last 2 years, in particular: Federico and Davide, for all those "beer breaks" because coffee was too mainstream; and all my nerdy friends for the best Warhammer evenings ever! Thanks to Lucia and Margherita for all our wine&chats nights and for all the support during these years at Uni.

I really need to thank the whole Amnesty Group for making me feel part of something bigger and raising me during my staying in Bologna. I'm thankful to the Disagio Gang: Mariuz, Mati&Mari, Silvi and Nella for every moment shared together: these years wouldn't have been the same without your company. I am also thankful to Eleonora: we shared our thesis period without killing each other, so we have been a great team!

Then I want to thank three VIPs: my flatmates Sonia, Valentina and Giulia for turning our house into a *Camping*... because with its mess, filth, overall chaos and lots of *disagio* was the perfect home to live, feeling like a weird, little family. In particular, thanks to Sonia for always being the only constant thing in these years.

The most important 'thank you' is for two people:

– Jessica: for listening to all my stupid ideas, projects and indecisions and for always supporting me and even my totally mad thoughts about life. Thank you for all the advice, for all the texts, all the memes and all the songs. You are the only one that doesn't make me feel totally crazy and so with you I can always just be myself.

– Antonella: for all our shared paths, now thanks to you I know I can overcome every climb. Then, thanks for all the speeches about chief systems and life: you have always helped me to work out my problems and to understand myself better than how I could do on my own. I really owe you a thousand beers, *vez*!

With her I need to thank Giada for every step during the *"Via degli Dei"* and every step during these months and Jacopo for all our swagging time together. Thanks to the three of you for all the *calcino* nights and for all the parties: you made my last university months more special than I could ever desire. Thanks for all the laughters, craps and mocks: I love you, asterisks!

* * *

And last but not least, the biggest acknowledgement goes to everyone – some of them just named before – who shared a trip with me: I think that whoever is tired of traveling is tired of living and there is nothing deeper than sharing something like this. So, thank you for being a part of important moments like bringing a backpack under a strong rain, sleeping in a cold station, riding a bike for miles, running not to lose a train, listening to the right playlist during a road trip, watching a sunset or a sea storm and sharing the silences, but most of all thanks for wondering and wandering.

"Not all those who wander are lost"

J.R.R. Tolkien